

REVIEW ARTICLE OPEN



Chemical vapor deposition-grown nitrogen-doped graphene's synthesis, characterization and applications

Geetanjali Deokar¹✉, Junjie Jin¹, Udo Schwingenschlögl¹ and Pedro M. F. J. Costa¹

The physical properties of carbon materials can be altered by doping. For instance, the electronic properties of graphene can be modulated by controlling the substitutional doping of the carbon lattice with N. In addition, C–N bonding configurations with three ring types are recognized: pyridinic-N, pyrrolic-N, and graphitic-N. Controlling the type and relative density of various types of substitutional N is an important objective that requires an extremely high level of precision when the atomic lattice is constructed. This control can be accomplished only via bottom-up methods, such as chemical vapor deposition (CVD). The number of reports on N-doped graphene (NDG) grown via CVD has increased over the past decade, but a reliable wafer-scale production strategy that can realize the desired atomic-precision growth of NDG is still lacking. To identify the most promising strategies and analyze the consistency of the results published in the literature, we review the CVD growth and characterization of two-dimensional NDG and two of the most popular applications of NDG films: field-effect transistors and energy storage devices.

npj 2D Materials and Applications (2022)6:14; <https://doi.org/10.1038/s41699-022-00287-8>

INTRODUCTION

Graphene is a two-dimensional (2D) structure in which sp^2 -hybridized C atoms are densely packed into a benzene-ring structure. Graphene exhibits ultrahigh mobility ($\sim 200,000 \text{ cm}^2 \text{ V}^{-1} \text{ s}^{-1}$)¹, broadband optical absorbance (2.3%) in the visible range, a large Young's modulus of 1 TPa, high thermal conductivity at room temperature ($\sim 5000 \text{ W/mK}$)², and large surface area ($2630 \text{ m}^2/\text{g}$)³. These extraordinary properties have sparked great interest in using graphene in applications, such as sensors^{4–7}, conducting channels^{8,9}, nanoelectronics¹⁰, flexible electronics¹¹, electromagnetic interference shielding¹², and energy storage^{13–16}.

Nonetheless, the zero bandgap of graphene impedes the development of graphene-based nanoelectronic devices and battery applications^{17–21}. Intrinsic graphene properties can be extended via bandgap tuning; thus, researchers have doped pure graphene with heteroatoms, molecules, nanoparticles, chemicals, adsorbates, and impurities^{22,23}. Heteroatom dopants can be electron donors (n-type) or electron acceptors (p-type). Among the heteroatoms explored to date are the N (n-type)^{17,24–27}, B (p-type), P (n-type)²⁸, S (p- or n-type)^{29, 30}, F³¹, Si (p-type), and Ge^{19,22,32–38}. Elements with larger atomic radii than C, such as S, Si, and Ge, can replace one or two C atoms^{19,22,32–38}. Moreover, halogen atoms (F, Cl, Br, and I) form ionic or covalent bonds with graphene, albeit with varying degrees of halogenation^{31,36,37,39,40}. Both B and N, the neighboring elements of C on the periodic table, easily substitute C in the graphene lattice, resulting in p- and n-type doping, respectively^{22,24,27}. As a dopant, N is more popular than B because it is more easily substituted into graphene²⁴. In particular, N has five valence electrons in the 2s and 2p atomic orbitals, which could form strong bonds with C atoms²⁴.

In addition, N-doped graphene (NDG) is widely applied in electronic devices^{26,41}, sensors^{42–44}, solar cells⁴⁵, enhanced catalysis^{46–52}, energy conversion, and storage^{49,53–55} (Fig. 1). However, most NDG-related reports consider the effect of the overall N-dopant concentration on device performance. Further, detailed studies focusing on the role of each type of C–N bonding

configuration and N-dopant location are needed, as demonstrated by a few researchers (e.g., Wei et al. demonstrated NDG with graphitic-N configuration use for application in field-effect transistors (FETs)⁵⁶). In NDG, the N-dopant bonding configurations are of three types: graphitic-N (sp^2 hybridization), pyridinic-N (sp^2 hybridization), and pyrrolic-N (sp^3 hybridization)^{26,32–35,56–58}. Each type of N-doping configuration affects the device performance in a specific way⁴⁹. Therefore, an appropriate synthesis approach that controls the N-doping configuration and N content for a specific device is in high demand.

Several NDG synthesis methods have been developed to date⁵⁹. These methods produce NDG with varied configurations, such as a different number of graphene layers and the type/distribution of N atoms. Moreover, they have distinct advantages and disadvantages regarding precursor costs, the overall process, thickness control, shape, defect size, reproducibility, and production scale. Some NDG synthesis methods use graphene flakes or graphene derivatives (graphene oxide, GO, or reduced GO) for scalable NDG production (Table 1). Although defects in graphene derivatives facilitate the doping process¹⁸, the end product is primarily synthesized in powdered form¹⁵. Controlling the defect sites (and hence the doping) in batch-to-batch samples of graphene derivatives is a challenging task⁶⁰. Direct thermal annealing of graphene derivatives during N doping causes irreversible stacking of the graphene sheets due to strong π – π interactions. To circumvent these problems, NDG can be grown using the chemical vapor deposition (CVD) process. To balance the cost-quality tradeoff of 2D NDG synthesis, the CVD method is more suitable than annealing¹⁶, physical vapor deposition⁶¹, pyrolysis^{62,63}, arc discharge^{27,64,65}, hydrothermal^{61,66,67}, and solvothermal^{21,68,69} syntheses (Table 1).

In FETs or battery applications, NDG is usually synthesized as a 3D network of 2D materials functionalized by additional moieties, such as metal nanoparticles⁷⁰, or post-processing using solvents, plasma, heat, or another physical process. A few excellent reviews on NDG have been published in the last decade^{20,32,33,57,59,71,72}.

¹King Abdullah University of Science and Technology (KAUST), Physical Science and Engineering Division, Thuwal 23955-6900, Saudi Arabia.

✉email: geetanjali.deokar@kaust.edu.sa

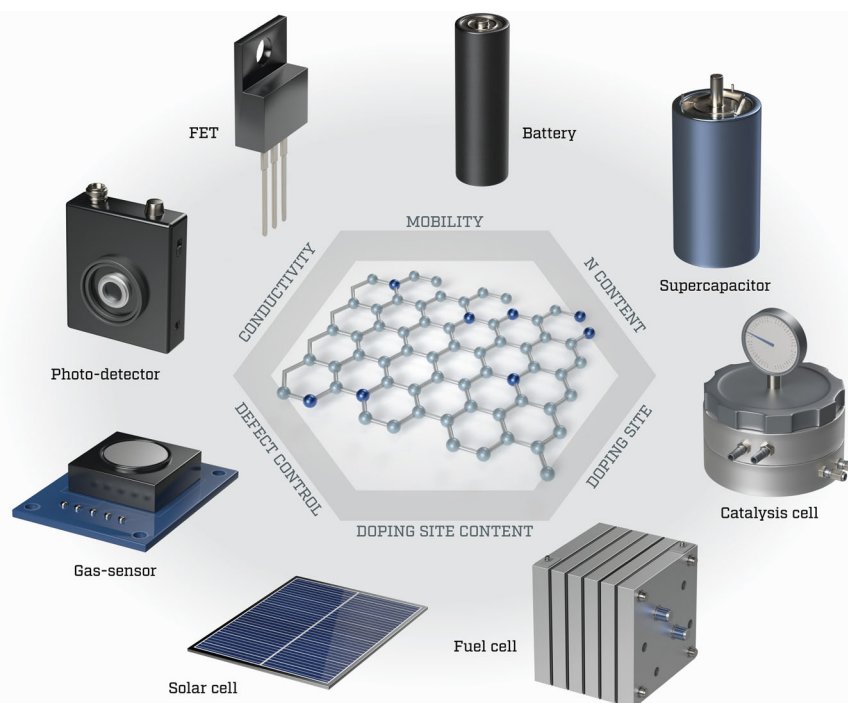


Fig. 1 Structure and applications of NDG. The gray hexagon in the center displays a molecular model of the N-doping configurations in a graphene lattice (gray and blue denote C and N atoms, respectively). Surrounding the NDG model expresses the properties of NDG needed in applications. The outermost circles enclose typical NDG applications with representative images (e.g., the field-effect transistor, etc.).

However, to our knowledge, a comprehensive review of CVD-grown 2D NDG is currently lacking. Recently, Ullah et al. reviewed the process and applications of 3D graphene modified with several dopants via CVD⁷². Focusing on graphene synthesis processes, Ikram et al. compared the uses of various carbon nanomaterials (3D networks) in battery applications²⁰. Wang et al. summarized various doping methods and applications of the resulting products³³. Still, the many challenges associated with controlling the N location and concentration in the graphene lattice, necessary for specific applications, have been overlooked.

We review the growth processes and characterization of CVD-based NDG, along with the quality consistency of the as-produced 2D material. The significance of controlling the N-doping configuration and using a straightforward CVD method is emphasized. Finally, we survey the current experimental and theoretical insight into FETs and energy storage applications based on as-grown NDG.

CHEMICAL VAPOR DEPOSITION OF N-DOPED GRAPHENE FILMS

Although CVD promises a reproducible and controlled high-quality synthesis of graphite/graphene thin films, at a large scale and low cost^{4,11,37,73–75}, fabricating reproducible wafer-scale 2D NDG with controlled properties remains challenging (Table 2)¹⁸. In addition, NDG synthesis via the CVD approach (Fig. 2) can employ a wide range of C- or N-containing precursors, either during graphene growth (in the same system, i.e., in situ) or afterward (i.e., ex situ treatment)^{34,35,53}. The N-dopant content of NDG, synthesized in or ex situ, ranges from 0.2 to 16 at.%^{32–35,46,56}. The ex situ synthesis properly controls the C–N bonding configuration⁷⁶ and is sometimes preferred due to its lower cost, higher reliability, and increased throughput¹⁷.

The CVD approach for N doping can occur via surface-charge transfer or, more commonly, via substitutional doping^{18,28,37}. In surface-charge transfer doping, metal atoms and gas molecules are adsorbed to the substrate;^{4,17,18,75} however, the electronic

properties of the resulting materials are unstable in the long term³⁷. Substitutional doping, which incorporates covalently bonded heteroatoms into the graphene lattice, stabilizes the material but degrades the extraordinary properties of graphene^{34,35}. Ideally, the performance enhancement should not disturb the intrinsic properties of graphene.

To study and control N doping in graphene, 2D NDG grown via CVD is eminently suitable, along with zero-dimensional⁷⁷ and 3D-NDG forms^{64,78} which are commonly produced using other synthesis methods. The CVD routes include thermal CVD^{25,26,56}, plasma-enhanced CVD^{34,79,80}, radio-frequency (RF) or microwave (MW) plasma CVD⁸¹, and electron cyclotron resonance CVD. Direct growth via plasma CVD on a dielectric substrate (e.g., glass or SiO₂/Si) has been reported, but the as-produced NDG crystals are small with a high density of defects (N–O and C–O bonds) and low electron mobilities^{34,79–82}. Thermal CVD produces NDG with significantly fewer defects and high electron mobilities^{25,26}. Recently, NDG with few defects and high charge carrier mobility has been obtained via the combination of plasma and thermal CVD⁸³. Table 2 compares the NDG growth methods developed in the most recent decade. Overall, the CVD NDG growth can be classified into two broad categories (see Fig. 2)^{14,26,32,33,46,81,84,85}.

1. In situ growth: N-containing gas/plasma treatment during the graphene growth or immediately after.
2. Ex situ growth: Post-growth N-doping treatment of as-made graphene.

In the in situ CVD approach, the NDG is usually grown on a transition metal catalyst (e.g., Cu or Ni). Similar to CVD graphene growth^{4,75}, a reactive mixture containing the C and N precursors is introduced at the growth temperature (~700–1000 °C)^{26,35,44,53,56,86}. These precursors dissociate on the surface of the catalyst, and NDG forms via the organization/precipitation of the C and N atoms. When the precursors are gases (e.g., CH₄ or C₂H₄ as the C source; NH₃ or N₂ as the N source), the amount of N dopant is varied by adjusting the flow rate, the ratio of the C and N precursor gases, and processing time^{46,56,80,85}. The N content is usually low (0.2–6 at.

Table 1. Typical NDG growth methods (advantages, disadvantages, and target applications).

Methods (N at. %)	Final product, precursors	Advantages	Disadvantages	Target applications	Few example references
CVD; (0.2–16.7)	mono-, few-layer graphene, N source: CH ₄ , C ₂ H ₂ , N ₂ , NH ₃ , pyridine, etc.	controlled quality and layer number, cm ² samples, processes of few hours, can be used as a model system to understand doping mechanism and doping site control	elevated to high-temperature requirements, sophisticated instrumentation, low-yields, needs transfer on a non-conducting substrate, quality degradation during transfer	FET, optoelectronics, photodetector, Li-ion battery	Wei, Nano Lett. 2009 ⁵⁶ ; Reddy et. al. ACS Nano, 2010 ⁵³
Annealing; (2.4–10)	graphene derivatives, N source: NH ₃ , N ₂ H ₄ , N, melamine, urea	use of commercially available powdered graphene materials, high N content, gm scale	treatment at elevated temperature, partial functionalization occurs, difficult to control N-doping type configuration	fuel cell, Li-ion battery, catalysis	Qiu, Nano letter, 2014 ¹⁵ ; Cai, Electrochimica Acta, 2013 ¹⁶
Arc discharge (1–3.5)	graphite, N source (gas/liquid): NH ₃ , pyridine, etc.	good for basic physics understanding experiments; high mobility values due to controlled N doping, use of gaseous/liquid N-sources	low N content, few-layered flakes (~1 μm), high precision instrument required, energy-intensive processes	FET, capacitor	Panchokarla, Adv. Mater. 2009 ⁶⁵ ; Pham, Adv. Fuct. Mater. 2019 ⁶⁴
Hydrothermal (10–16)	graphene derivatives, N precursor (solutions): NH ₃ , NH ₄ OH, urea, polypyrrole, etc.	high N content, low-cost, low-temperature (~200 °C) heat or microwave treatments, large-scale production—gram to tons scale, N-doped quantum dots	flakes or powder form, no control on layer number and flake size, weak inter-junction connections, lengthy processes, limited batch-to-batch quality control, crumpled sheets	catalysis, batteries, fuel cell, supercapacitor, cell and tissue imaging	Long, Langmuir. 2010 ⁶⁷ ; Sun, RSC. Adv. 2012 ⁶⁶
Pyrolysis (2–8.35)	graphene derivatives, N source: polyaniline, urea, melamine, polypyrrole, etc.	large-quantity production	graphene derivatives elevated temperature annealing, porous and powdered material, defective, lengthy processes, residual C–O bonds, and oxidized N–O bonds presence	electrodes for ORR, fuel cell	Lin, Adv. Energy Mater. 2012 ⁶²
Solvothetmal (4–28.1)	graphene derivatives, N-Resin, CoCl ₂ , Li ₃ N + CCl ₄ annealing in Ar + Li ₃ N, etc.	high N content, gm scale	annealing at elevated temperatures, lengthy processes, powdered material, crumpled sheets, no control on graphene layer number and flake size	batteries; fuel cell, catalysis, supercapacitor, microwave absorber	He, J. Mater Chem A, 2013 ²¹ ; Bai, Hydrogen Energy, 2013 ⁶⁸ ; Deng, Chem. Mater. 2011 ⁶⁹

Table 2. Examples of NDG growth using the CVD method.

CVD Type; Substrate; Sample size (cm ²)	T (°C); Growth time (min)	Precursors; Pressure (mbar)	N at.% (XPS)	Application and remarks	Ref. (1 st author, Journal, year)
AP-CVD Cu foil (127); 6.4	300–1000; ~few hr	pyridine, H ₂ ; 1000	1.6 (1.8 –TEM)	two-step, oxidized N, polymer-assisted wet transfer using FeCl ₃ etchant. claimed low-temperature growth method for direct synthesis on a device, however, annealed Cu foil at 1000 °C	Son, Carbon, 2020 ²⁶
HF + PE-CVD Quartz; 6.7	850; 9	C ₂ H ₂ , H ₂ , N ₂ ; 0.1	3	defective graphene, electricity generation device—320 mV, better than pristine graphene, three types of N-doping, transparency ~90%—for high N ₂ flow (20 sccm), N-doped graphene flakes with amorphous carbon	Zhai, J. Mater. Chem. A 2019 ³⁴
PE-CVD; SiO ₂ /Si	175	C ₂ H ₂ , NH ₃	0.7	FET, pyridinic-N, catalyst-free growth, low-temperature, bright atoms attributed to N in STM images	Wei, ACS Nano, 2015 ⁸²
Thermal CVD; Ni	1100; 12	Monoethanolamine, N ₂ ; NM	2.9	one to ten graphene layers, high substrate temperature, liquid source, three types of N-doping configurations exist, need of two heating zones	Bao, Mat. Lett. 2014 ⁸⁹
LP-CVD; Cu	900;>60	C ₂ H ₂ , H ₂ , NH ₃ , He; 1.3	16	two-step process, pure pyridinic-N, raise of the density of π states near the Fermi level and the reduction of work-function, electrochemical measurements, pyridinic-N not a promoter of ORR activity, electrodes for ORR studies	Luo, J. Material Chem., 2011 ⁴⁶
HW-CVD; Cu foil (25); 4	1000; 20	Ar; pyridine; 6–8	2.4	graphitic-N major, highly toxic N source	Jin, ACS. Nano 2011 ⁸⁷
AP-CVD; Cu foil (25); <4	850; 10	Ar, H ₂ , CH ₄ , NH ₃ ; 1000	0.25	in situ post NH ₃ treatment, substitutional N doping, STM imaging, N doping- 2.53 × 10 ¹² N atoms per cm ² , TEM images same as pristine graphene -no structure change	Ly, Sci. Rep. 2012 ⁷⁹
Thermal CVD; Cu foil (25); ~1.5	950; 500	Ar, H ₂ , NH ₃ Hexane, Acetonitrile, NM	9	LIB battery anode, direct growth on Cu current collector, major pyridinic-N, reversible LIB capacity higher for N-doped graphene than graphene	Reddy, ACS Nano 2010 ⁵³
Thermal CVD; Cu foil; <4	800; 10	Ar, H ₂ , CH ₄ , NH ₃ ; NM	8.9	graphitic-N major, FET, N-doped graphene better FET on-off ratio than pristine graphene. I _g /I _b ~0.5 m, many wrinkles and broken areas, not fully graphene-FLG and MLG presence	Wei, Nano Lett 2009 ⁵⁶

CW cold wall, HW hot wall, AP atmospheric pressure, PE plasma-enhanced, T temperature, NM not mentioned. Other abbreviations described in the main text (e.g., NDG, CVD, IG, ID, STM, TEM, FET, FLG, MLG, LIB)

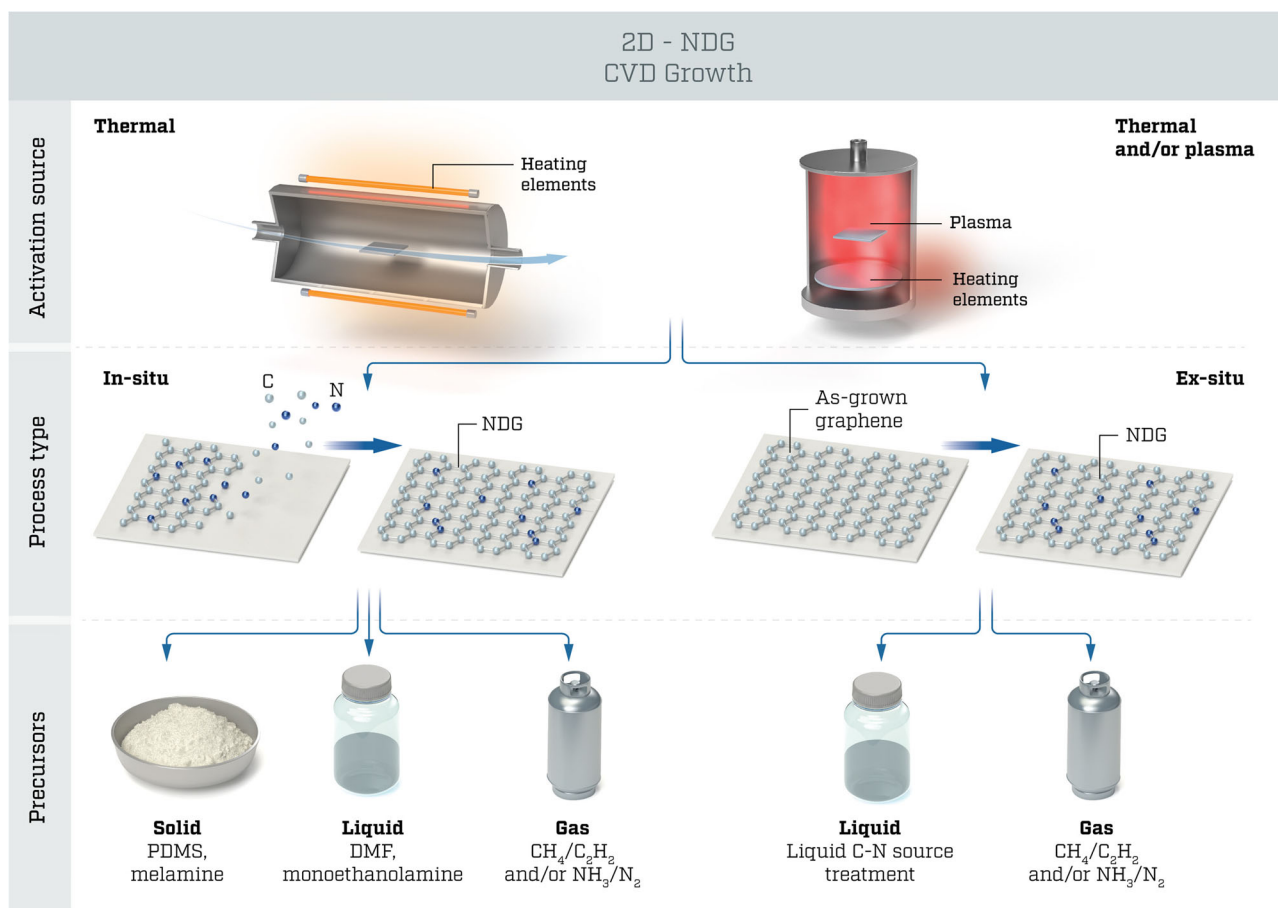


Fig. 2 Tree diagram of NDG growth via different CVD approaches categorized by type. (1) activation source (thermal, plasma, or both), (2) type of process (in situ or ex situ), and (3) source material type (solid, liquid, or gas).

%) but a few reports have claimed otherwise (9–16 at.% sourced from NH_3 ; see Table 2).

NDG has also been grown using solid/liquid organic precursors, such as pyridine^{26,46,58,87}, acetonitrile⁵³, CH_3CN ⁸⁸, dimethylformamide³⁵, melamine, and monoethanolamine⁸⁹. However, in most of these reports, the quantity of liquid precursor was not mentioned or is vaguely stated. Therefore, their reproducibility is uncertain. In addition, solid/liquid N precursors³⁵ yield a high O content in the form of C=O and C–O or N–O bonds (as detected via x-ray photoelectron spectroscopy [XPS])⁸⁸, which lowers the quality of the resulting NDG material. Among the solid/liquid precursors, the sublimation point of melamine is too high (343 °C), and acrylonitrile (containing C–C, C=C, and C≡N bonds) cannot form graphitic-N-type when heated to a temperature of >500 °C⁵⁷. In contrast, pyridine has bond energies similar to graphitic-N-type, inducing the formation of NDG with dominant graphitic-N-type bonds that do not significantly degrade the graphene lattice²⁶. However, pyridine is highly flammable (with a flashpoint of –21 °C) and toxic. Therefore, its use requires extreme care and the CVD growth must proceed in well-regulated conditions.

Thus far, catalytic Cu foils (rather than Ni) are preferred to obtain controlled 2D NDG, a trend that follows the CVD graphene processes²⁶. As the solubility of C in Ni is high⁹⁰ (C solubility in Cu is 0.03 at.% at 1000 °C⁹¹, while in Ni is 0.29 at.% at 700 °C and 0.9 at.% at 900 °C^{92,93}), C atoms diffuse in the Ni substrate during the growth step. Knowingly, these C atoms out-diffuse and form multilayer graphene during the cooling step^{94,95}. Similarly, if N is implanted in the Ni lattice (the diffusion coefficient of N in Ni is $4.46 \times 10^{-13} \text{ m}^2/\text{s}$)⁹⁶, the N atoms out-diffuse to the Ni surface and N atoms can become trapped in the graphene lattice, forming

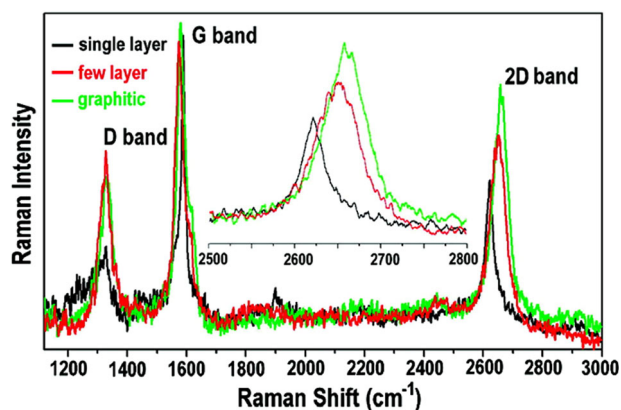
NDG during the cooling step. This hypothesis was experimentally confirmed in the ultrahigh-vacuum growth of NDG on a Ni (111) single-crystal substrate, which extended over a few square nanometers⁷⁶. Interestingly, these authors pretreated the substrate under a porphyrin flux prior to graphene growth, achieving precise control of the C and N quantities. Similarly, Zhang et al. performed vacuum annealing on a Ni/B/SiO₂/Si substrate with trace elements (C, N, etc.) present in the reactor. Upon cooling, an analog of NDG was formed ($N = 0.6\text{--}2.3 \text{ at.}\%$). The C atoms were trapped in Ni while N was trapped in the B films, thus segregating the C and N⁹⁷. It would be pertinent to test these experiments at wafer-scale and under thermal CVD conditions (low-to-high pressure and elevated temperatures).

Ex situ CVD processes include the post-treatment of previously grown graphene layers¹⁴ or flakes^{17,79,81,98}. The ex situ treatments are similar to those of thermal annealing (Table 1). Note that, in the literature, thermal annealing often refers to the processing of powdered graphene derivatives (3D networks)⁵⁹; these are outside the scope of this review. The ex situ growth of NDG is uniquely advantageous for simultaneous device production^{17,79}.

We noticed a considerable variation among the N-doping environment of CVD processes (Table 2). The variable parameters include activation source (heat, plasma, or both), treatment time (few seconds to a few hours), chamber pressure (from ultrahigh-vacuum to atmospheric pressure), substrate temperature (450 to 1040 °C), and catalyst material thickness (a few tens to a few hundred micrometers). Such scattering offers little value as each of these parameters can control the quality of the as-produced NDG material. In fact, few teams have claimed dominant N-doping configuration (graphitic-N, pyridinic-N, or pyrrolic-N-type) as a

Table 3. Summary of various characterization techniques used for CVD-grown NDG (the abbreviated technique names are defined in the main text, e.g., - SEM).

Characterization techniques	Sub-technique (areas of information)	Type of information
Microscopy	SEM (cm ²)	larger area uniformity, surface defects (tears, folds, cracks, residues, etc.)
	TEM (nm ²)	structure, contaminations, direct view of N inclusion
Scanning probe microscopy	AFM (μm ² -nm ²)	thickness, roughness
	KPFM (μm ² -nm ²)	surface potential
	STM (nm ² , surface sensitive)	atomic structure, direct view of N inclusion
Spectroscopy	Raman spectroscopy (μm ²)	structure and chemical composition
	XPS (μm ² , surface sensitive)	chemical composition, contaminations
	ARPES (nm ² , surface sensitive)	band-structure

**Fig. 3 Raman spectroscopy results.** Raman spectra of NDG with different numbers of layers. The inset is a zoomed-in view of the 2D band (reproduced from⁵⁶ with permission from the American Chemical Society).

result of fine-tuning the CVD parameters (Table 2)⁴⁶. For instance, Li et al. obtained major pyrrolic-N-type NDG growth by setting a high substrate temperature (1000 °C), which inhibits the pyridinic-N-type configuration⁸⁵.

To date, the areas of NDG films grown via CVD are on the scale of square nanometers or square micrometers^{26,32,81,99}. Future studies should target the growth of wafer-scale NDG with structural and thickness uniformity^{33,99}. In particular, the NDG growth process must be systematized to clarify the relationship between the process parameters and the N lattice sites as well as their bonding configuration^{26,32,33,56,76}.

N-DOPED GRAPHENE CHARACTERIZATION

To characterize NDG, researchers employ various analytical tools^{18,71}. Unlike the previous reviews^{20,32,33,57,59,71,72}, we constrained the characteristics of CVD-grown NDG to the number of layers, overall texture/structure, surface chemistry, and a few other physicochemical attributes (summarized in Table 3).

Optical spectroscopy

Raman spectroscopy is a powerful nondestructive tool that evaluates the crystalline quality, number of layers, and doping level of NDG^{100,101}. Figure 3 presents a typical Raman spectrum of an NDG sample. The spectrum exhibits four peaks in 1000 to 3000 cm⁻¹ range, one each in the D band (~1351 cm⁻¹), G band (~1590 cm⁻¹), D' band (~1629 cm⁻¹), and 2D band (~2696 cm⁻¹)^{35,44,53,56,81}. Some studies have reported a shoulder peak in the D' band, associated with defects in the graphene

lattice^{46,53}. The NDG growth can be detected via Raman spectroscopy, as the G and D bands are sensitive to chemical doping¹⁰¹.

The D band observed in graphitic C is a disorder-induced feature. The heteroatoms disrupt the graphene lattice symmetry, enhancing the intensity of the D band in NDG samples^{14,35,37,56,57,88} compared with that of pristine graphene⁷⁵. In Raman mapping studies⁴⁴, Luo et al.⁴⁶ and Xu et al.¹⁷ reported an enhanced D peak resulting from increased defects in an NDG lattice over large areas (6 × 4 μm). Using Raman mapping, they revealed that the incorporated N formed a domain rather than a uniform distribution through the lattice. This finding was endorsed by time-of-flight secondary ion mass spectrometry scanned over a few tens of square micrometers.

In the literature, the D band to G band intensity ratio (I_D/I_G) of CVD-grown NDG ranges from 0.87 to 1.0 (Table 2), which is higher than that in CVD-grown graphene or graphite thin films^{4,73-75}. Ito et al. demonstrated that the I_D/I_G ratio in NDG largely depends on the selected C and N source gases with or without the use of H₂⁸⁶. They found lower I_D/I_G values at a relatively higher H₂ flow (>100 standard cubic centimeter (minute)) or growth temperature (>800 °C), which they attributed to fewer C-N bonds and a more ordered graphene lattice. At low N-doping concentrations (<2 at. %), the G and 2D bands of the NDG samples are narrow and symmetric, similar to those of pristine graphene⁸².

Upshifted G and 2D bands are a common feature of substitutional N doping in graphene lattices^{46,81,85,101}. In contrast, adsorbed n-type-doped heteroatoms feature a downshifted G band. This downshift was reported by several groups employing ex situ graphene processing¹⁷. Moreover, the full width at half maximum of the D and G bands was greater in the spectrum of pyrrolic-N NDG than in the spectra of graphitic-N⁵⁶ and pyridinic-N-type NDG^{46,53}, at the same doping concentration.

From the above studies, a higher-intensity D band is a valuable fingerprint of NDG. However, as other defect types can increase the D-band intensity, further confirmation of N doping via other techniques is required. Several groups have claimed NDG growth after measuring the Raman spectra at a few points on the sample, which is insufficient. Other studies have supported NDG growth using other characterization tools, which is highly recommended for confirming the layer number, crystalline quality, and N-doping content of NDG samples.

Other optical spectroscopic techniques, such as Fourier-transform infrared spectroscopy⁸¹, ultraviolet (UV)-visible spectroscopy⁸¹, and THz time-domain spectroscopy⁸⁵, are seldom used in NDG characterization; thus, these are not discussed in detail, here.

Surface analysis techniques

To understand the pathway of N doping, we probe the elemental composition and chemical bonding of the doped N atoms in NDG. The most powerful tool for this purpose is XPS, which provides a surface-sensitive chemical analysis to depths of 1 to 10 nm. A

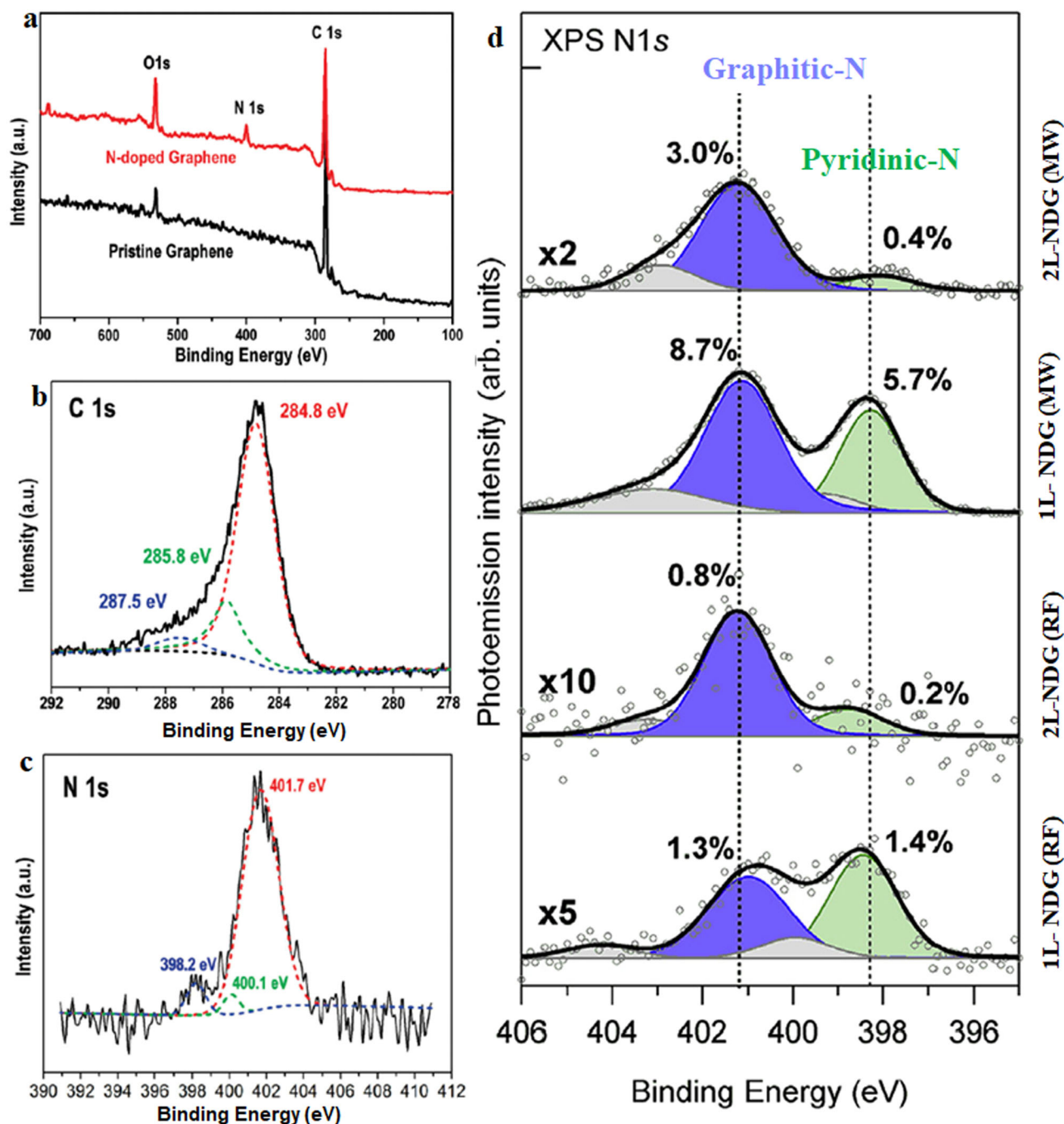


Fig. 4 X-ray photoelectron spectroscopy results. **a** Survey spectra and **b, c** High-resolution core-level C1s and N1s spectra of NDG obtained via thermal CVD (reproduced from⁵⁶ with permission from the American Chemical Society), **d** N1s spectra of NDG samples treated with microwave (MW) and radio-frequency (RF) plasmas. The numbers state the N at.% deduced from spectral analyses of graphitic-N and pyridinic-N (reproduced from⁷⁹ with permission from Elsevier).

typical XPS survey spectrum of an NDG sample is scanned over the 200 to 450 eV range of binding energies. The N content in the NDG is estimated from the intensity ratio of the N1s (~400 eV) and C1s (~284 eV) peaks. The N configurations can be determined from high-resolution C1s and N1s spectra^{44,46,53,79,83}. Different C–N chemical bonding configurations manifest as several shoulder peaks in the core-level spectra. The C1s peak of an NDG sample can usually be deconvoluted into three components: (i) the major peak at a binding energy of 284.4 eV (sp^2 -hybridized C atoms in graphene/graphite)^{73,75}, (ii) a peak at 285–285.5 eV (sp^2 C bonded with N), and (iii) a peak at 286.5 eV (sp^3 C atoms bonded

with N)^{46,53}. However, many NDG reports do not present the C1s core-level spectra⁸⁶.

The N1s core-level spectrum also deconvolutes into several component peaks. Three main types of N-doping configurations are frequently reported⁷⁶. Pyridinic-N and pyrrolic-N may lie at the edge of the lattice, and graphitic-N forms by replacing C in the graphene lattice. The binding energies of these C–N bonding configurations were found at 398.1–399.3, 399.8–401.2, and 400.5–402.7 eV, respectively^{53,76}. Nitrilic-, pyrazole-, and oxidized-N-type bonding have also been reported^{46,79}. Lin et al. post-treated graphene/SiC samples in NH_3 plasma and found that

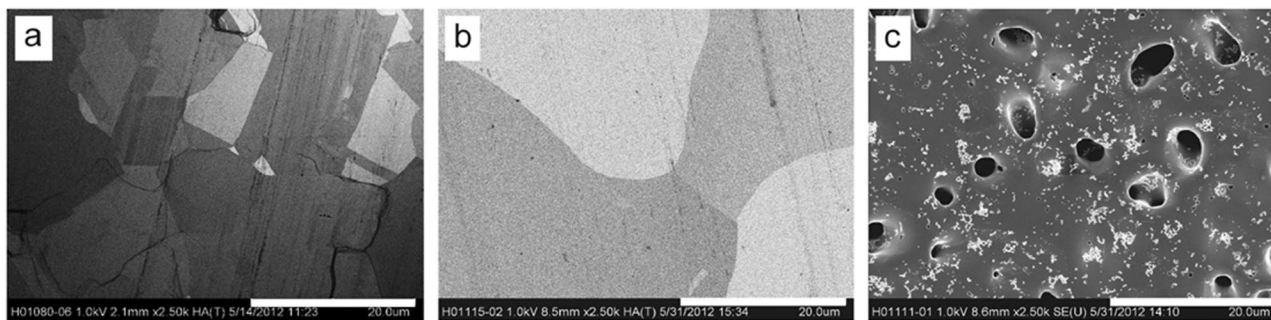


Fig. 5 Scanning electron microscopy results of N-doped graphene. SEM images of N-doped graphene grown on Cu substrates using different precursor treatments (under an H₂ flow during growth). Scale bar in each image is 20 µm: **a** CH₄, **b** pyridine, and **c** nitroethane (reproduced from⁸⁶ with permission from the American Chemical Society).

the insertion of N species depends on the graphene thickness (Fig. 4b)⁷⁹. They reported that MW plasma yields a higher N doping in bilayer NDG than RF plasma. In addition, graphitic-N (3 at.%) dominated pyridinic-N (0.2 at.%) in bilayer graphene, whereas the pyridinic-N formation dominated in single-layer graphene. Thus far, NDG with pure pyridinic-N, pure pyrrolic-N, and pure graphitic-N doping configurations were reported by Luo et al.⁴⁶, Li et al.⁸⁵, and Wei et al.⁵⁶, respectively.

As a complementary technique to XPS, ultraviolet photoelectron spectroscopy (UPS) probes the doping types in graphene^{17,46,81}. Molecules absorb UV light and emit photoelectrons. The molecular orbital energies in the valence band are determined by measuring the kinetic energies of the released photoelectrons. Luo et al. probed the electronic structure of NDG via UPS⁴⁶ and discovered that pyridinic-N effectively modifies the valence band structure in graphene. The density of the p-doping states increased near the Fermi level, and the work-function increased by 0.2 eV from that of graphene. Xu et al. also observed a work-function difference of ~0.2 eV between NDG and pristine graphene from UPS measurements¹⁷. They confirmed a similar work-function difference between NDG and graphene using Kelvin probe force microscopy (KPFM).

Angle-resolved photoemission spectroscopy (ARPES) probes the electronic structure of graphene at the Fermi level near the K point in the Brillouin zone^{18,75}. The band structure of graphene can be determined from the energy dispersion as a function of momentum along the high-symmetry directions measured via ARPES^{75,98}. The Fermi level is located at zero binding energy, and the Dirac point is located near the Fermi level in pristine or doped graphene⁷⁵. For example, Lin et al.⁷⁹ reported a 450 mV Fermi-level shift in SiC n-type-doped NDG. Dopants (p- or n-type) in graphene are introduced from the doping and graphene substrate⁷⁵ or polymer residues that remain after the transfer process^{102,103}. Because the spectral densities of states measured via ARPES are extended in real space, this technique is insensitive to local resonances but determines the resonant behavior of N doping⁹⁸.

The above studies confirm that XPS reveals the doping content and N-doping configuration type, whereas UPS and ARPES detect the Fermi-level shift due to N doping. Other characterization techniques are necessary to confirm the N-doping levels and their effect on the local structural and electronic properties of NDG. These techniques are discussed in the following subsection.

Electron microscopy

Scanning electron microscopy (SEM) is routinely used to examine the morphology of various materials, including NDG. A beam of highly energetic electrons (with a few keV of kinetic energy) is scanned over the sample surface, and the secondary electrons (~50 eV) emitted from the sample produce an SEM image. Similar to graphene or graphite films^{73–75}, NDG is placed on a substrate

(Cu, Ni, SiO₂/Si, etc.) for SEM imaging. The number of NDG layers can be qualitatively correlated to the image color contrast^{74,81}. Using SEM imaging, Ito et al. investigated the effects of different C and N precursors on NDG growth (Fig. 5)⁸⁶. The NDG grew over a large area (a few cm²), similar to that of graphene; however, the nitroethane-grown surface was severely damaged. This technique is useful for global characterization, but the N-doping content and locations must be confirmed using the previously discussed techniques.

Local structural measurements (with areal coverages of squared nanometers to squared micrometers) can be performed with transmission electron microscopy (TEM). In preparation for TEM, the NDG is transferred to an amorphous C-coated Cu or Au TEM grid^{34,85}. In analysing NDG, researchers have compared the structural differences between pristine graphene and NDG samples³⁴. Son et al. directly observed substitutionally-doped N using atomically resolved high-resolution TEM (HR-TEM)²⁶. They applied a bandpass filter to capture clear images of the N atoms in the vicinity of C atoms. The substitutional N atoms were clearly imaged as high-brightness points in the graphene plane (Fig. 6a). The height profile of the HR-TEM image (dotted red line in Fig. 6a) abruptly increased for N atoms (Fig. 6b). The selected area electron diffraction (SAED) patterns of the same sample revealed single-crystal graphene without lattice breakdown (Fig. 6c).

The intensity of the diffraction spots of NDG was similar to that of pristine graphene, indicating that the crystalline quality was maintained after doping²⁶. The low N content (<3 at.% in graphene) yielded NDG with high crystalline quality^{26,44,87,97}. Techniques accompanying TEM imaging, usually elemental mapping via electron energy loss spectroscopy (EELS), confirm that N atoms are uniformly distributed in NDG samples (red spots in Fig. 6d)^{34,35}. From the EELS data, the N-doping amount was estimated as ~1.8 at.% (in a similarly grown sample, XPS yielded a similar N content of 1.8 at.%).

Graphene and NDG grown with plasma CVD result in ring patterns when examined by SAED, due to their polycrystalline structure (originates several hexagonal sets of spots)³⁴. The diffraction rings of graphene correspond to (002), (111), and (100) orientated nanocrystallites with interplanar spacings of 0.33, 0.26, and 0.21 nm, respectively³⁴. In the diffraction pattern of NDG, the absence of the ring corresponding to the (002) plane correlates with the decreased interplanar spacing of NDG³⁴. More structural TEM analyses of NDG produced with precisely controlled N-doping levels are required.

Scanning probe methods

Atomic force microscopy (AFM) can confirm the thickness (number of layers) of an NDG sample, similarly to graphene samples⁸¹. The UPS results have rarely been supported by KPFM, as discussed¹⁷. This subsection focuses on scanning tunneling microscopy (STM) and scanning tunneling spectroscopy (STS),

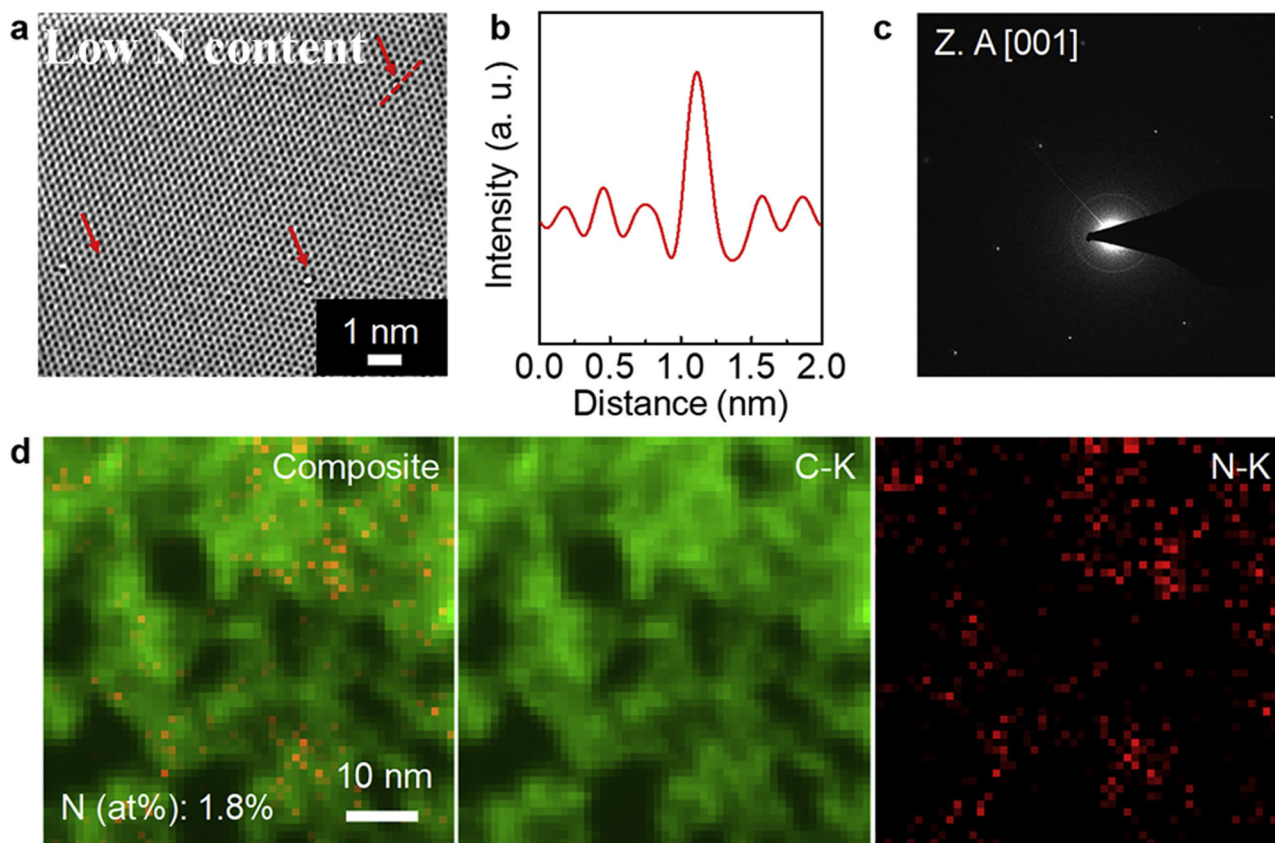


Fig. 6 Transmission electron microscopy imaging on NDG with low N content (<2 at.%). **a** Bandpass-filtered high-resolution TEM image, **b** height profile of the dotted red line in panel **a**, **c** selected area electron diffraction pattern, and **d** elemental mapping images using electron energy loss spectroscopy (reproduced from²⁶ with permission from Elsevier).

which provide significant information on the quality of an NDG material.

The local atomic structure of graphene around the N dopants can be scanned using STM^{76,84,98}. This method also controls and locates substitutional N-doping sites^{44,84}. Joucken et al. elucidated the electronic structure of NDG in a combined XPS, ARPES, and STM/STS analyses (Fig. 7a–e)⁹⁸. As the doping concentration increased from 0 to 1.1 at. %, the Fermi-level shift increased from 0 to 450 eV.

Recently, Lv et al. reported the topography of individually doped N atoms in a highly resolved STM image of graphene treated in situ using NH_3 in a two-step process (Fig. 7f)⁸⁴. They performed STM observations of samples transferred onto SiO_2/Si with unique double-substitutional N-doping sites (N_2^{AA}). In density functional theory (DFT) calculations, they further confirmed the occurrence of localized states in the conduction band induced by N_2^{AA} type doping. Thus with the use of STM technique, N-doping at atomic scale was evidenced.

STM locates the N doping with an atomic resolution over a sample surface scanned over areas in square nanometers⁷⁶. However, this technique not suitable to confirm whether the dopant is uniformly dispersed over large areas (approximately centimeters squares).

MODELING

DFT simulations are another critical tool for studying the properties of NDG, particularly the geometry and electronic properties. According to various theoretical studies, N doping can effectively increase the electron density of graphene while adjusting the

Fermi energy (E_f) level. Moreover, chemical properties can be adjusted via N doping⁸⁰.

The semiconducting behavior of NDG depends on the configuration type of N doping. Pyridinic-N and pyrrolic-N mainly form at the defects and edges of NDG, whereas graphitic-N forms at the replacement sites of C atoms. Therefore, NDG maintains high electron mobility similar to that of graphene¹⁰⁴. As the bond lengths of C–N and C–C are similar (1.41 and 1.42 Å, respectively), the pyridinic-N and graphitic-N doping types have little effect on the graphene structure, but the pyrrolic-N doping type undergoes a structural change from the original hexagonal lattice. Pyridinic-N is the most stable type for monovacancy, whereas pyridinic-N and graphitic-N energetically favor Stone–Wales and divacancy defects¹⁰⁵. In graphitic-N-type NDG, three σ -bonds form between N and its neighboring C atoms; one is involved in the formation of the π bond, and the last bond is partially involved in the π^* state of the conduction band. The resultant doping in graphene is n-type¹⁰⁶. In contrast, pyridinic-N and pyrrolic-N-type NDG form defect sites that withdraw electrons from graphene, inducing p-type doping¹⁰⁷.

APPLICATIONS

Among the many possible applications of NDG (Fig. 1), we focus on FET and battery technologies, which directly use CVD-grown NDG for nanoelectronics and storage, respectively. Both applications require further improvements in capacity and performance. Other applications require growth scaling and architectural modifications of CVD-grown graphene. These fields are excluded because listing all these would be excessively exhaustive. 2D NDG has been used in several studies on FETs¹⁷ and battery devices

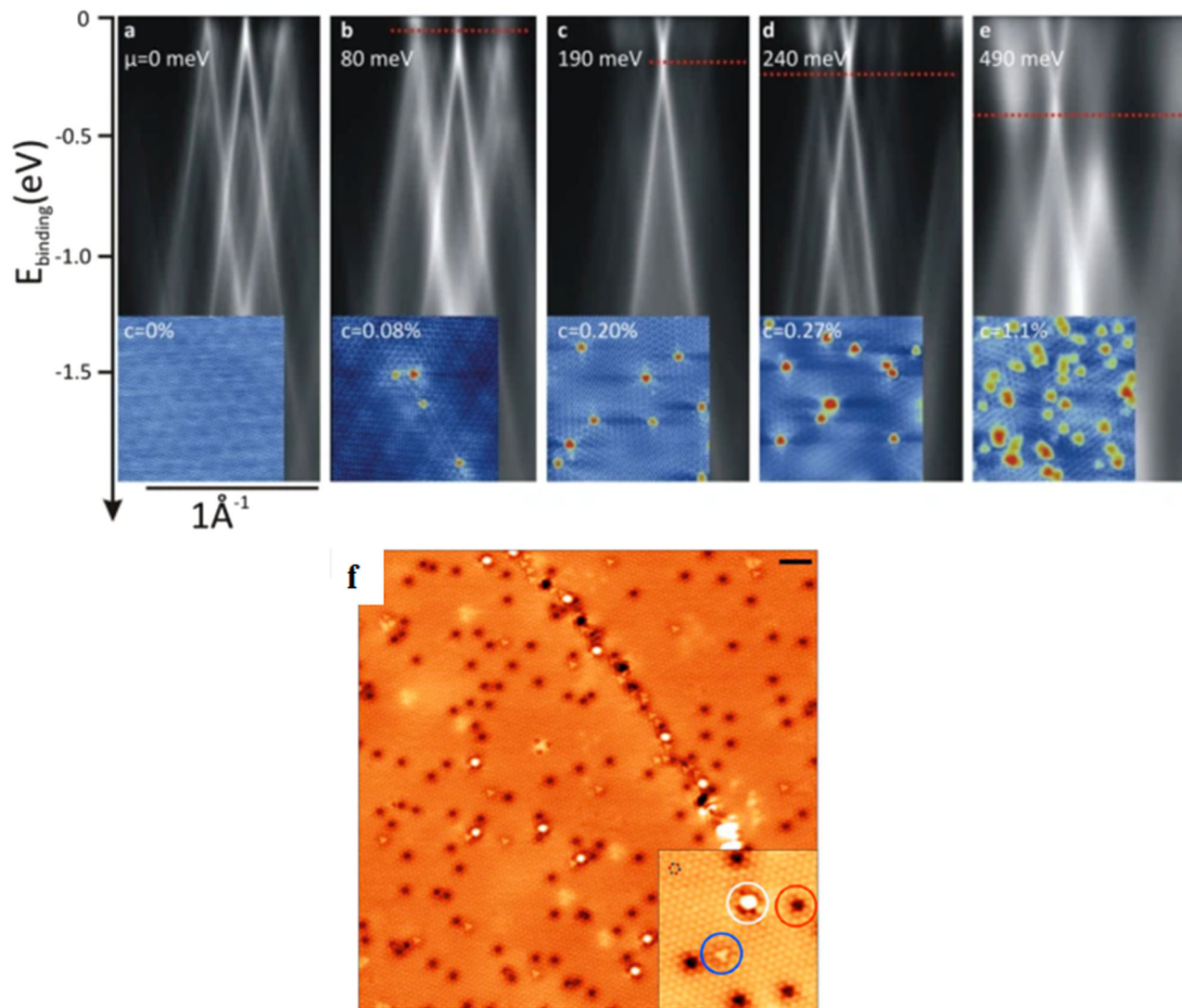


Fig. 7 Scanning tunneling microscopy and angle-resolved photoemission spectroscopy results. a–e ARPES spectra of samples treated for 0, 7.5, 15, 30, and 90 min. The Fermi-level shift ($\mu = E_F - E_D$) is stated on each spectrum. Insets present typical ($10\text{ nm} \times 10\text{ nm}$) STM images of the corresponding samples. The N dopants appear as red protrusions, and the N concentration (c) is given on each image (reproduced from⁹⁸ with permission from Springer Nature). f Low-temperature STM image acquired at 77 K. Several surface defects appear. Inset displays the three most abundant types of defects. Scale bars = 2 nm, $I = 2.0\text{ nA}$, $V = 0.2\text{ V}$ (reproduced from⁷⁶ with permission from Elsevier).

(Table 2)⁵³. The FETs require proper N-doping locations and low N content to avoid a drastic decrease in electron mobility and open a suitable bandgap, whereas battery applications benefit from a specific type of N-doping configuration, as detailed below^{19,53}.

Field-effect transistors

In reciprocal space, the valence and conduction bands of graphene intersect at two inequivalent points, providing a unique electric field effect and high conductivity. Graphene exhibits an ambipolar behavior where both the hole and electron carriers are transported perpendicular to its surface^{9,11,13,17}. The first high-speed FET based on graphene was prepared via the micromechanical cleavage of pyrolytic graphite¹⁰⁸. Since then, graphene and doped graphene-based nanoelectronics have been extensively researched. The effects of doping on the electrical properties of graphene can be investigated via electrical measurements in FET geometry (Fig. 8)^{25,97}. The NDG-based FET devices have a bandgap and exhibit a larger on/off current ratio and lower turn-on fields than pristine graphene^{35,38,57}.

The FETs are usually fabricated from CVD-grown NDG graphene transferred onto a SiO_2/Si substrate^{17,25,35,83}. The Cu or Au electrodes are deposited onto the patterned NDG film via thermal or e-beam evaporation^{9,17}. The NDG provides a conducting channel between the source and drain electrodes⁹. Xu et al. reported high mobility and a Dirac point shift of -140 V in NDG grown via an ex situ treatment of CVD graphene (surface-charge transfer type doping)¹⁷, whereas NDG grown using substitutionally-doped N exhibited lower mobility values^{56,58}. Wei et al. prepared bottom-gated FETs from NDG (with a significant graphitic-N configuration) and pristine graphene⁵⁶. They reported relatively lower mobility and a higher on/off ratio in NDG than in graphene⁵⁶. The lower mobility in NDG can be attributed to the disrupted symmetry of the graphene lattice due to the incorporated N atoms. The generated defects behave as scattering centers, reducing mobility and conductivity⁵⁸. The mobilities of NDG have reached values of 200 to $450\text{ cm}^2/\text{Vs}$, which are lower than the commonly reported mobilities of CVD-formed graphene (1000 to $5000\text{ cm}^2/\text{Vs}$)^{9,75,109,110} (Table 3). The mobility of NDG exceeds that of graphene doped with other

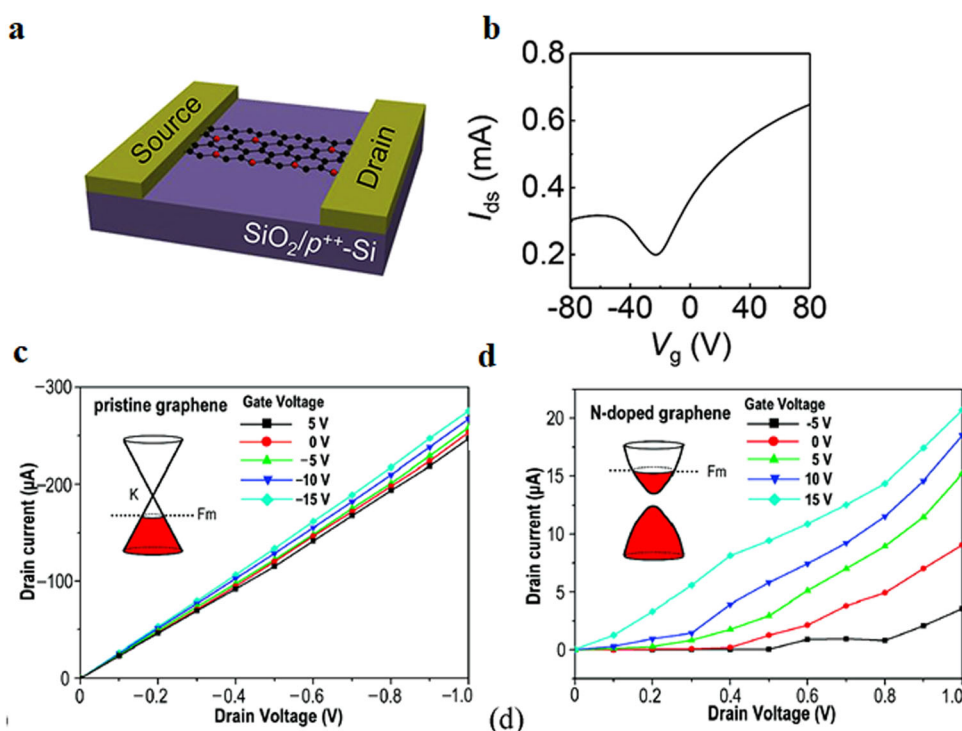


Fig. 8 **Electrical properties.** **a, b** Schematic of a field-effect transistor (FET) device and I - V_g characteristics of a NDG-based FET (reproduced from²⁶ with permission from Elsevier); **c, d** I_{ds} versus V_{ds} plots of graphene and NDG FET devices for various V_{gr} , where V_{gr} , I_{ds} , and V_{ds} denote the gate voltage, source-drain current, and source-drain voltage, respectively. Insets at the upper left of panels **c** and **d** are the presumed band structures of graphene and NDG FET devices, respectively (reproduced from⁵⁶ with permission from the American Chemical Society).

heteroatoms via CVD methods. For example, the mobility of graphene doped with 4 at.% of S is $270 \text{ cm}^2/\text{Vs}$ ²⁹.

Pyrrolic-N and pyridinic-N configurations generally have high defect densities, resulting in a lower graphene carrier conductivity and mobility than those of the graphitic-N configuration^{46,83}. Recently, Xu et al. developed a higher-mobility ($1150 \text{ cm}^2/\text{Vs}$) FET device in which the N dopants were adsorbed on bilayer graphene¹⁷. They postulated that the low defect densities in NDG substantially weaken the short-range scattering and improve mobility.

The bandgap in the semiconductor channel of conventional FETs should be at least 0.4 eV ¹¹¹. The NDG band structure has been calculated in DFT and ab initio simulations. Mukherjee et al. showed that 12.5 at.% N doping in graphene reduces the Dirac cone shift below the E_f by 1.5 eV with finite splitting¹¹². Below E_f , the π , and π^* bands are contributed by the p_z orbitals of C and N, respectively (Fig. 9a). By increasing the N-doping concentration from 3.13 to 12.5 at.%, Olaniyan et al. increased the bandgap of NDG from 0.21 to 0.6 eV ¹¹³, meeting the requirements of FET channel materials (Fig. 9b, c). As N atoms are more electron-rich than the resident C atoms, the Fermi level moves significantly above the Dirac point, resulting in n-type semiconductor materials.

A significant scope remains for enhancing FET results by controlling the percentage and configuration of the N dopant. In future studies, the uniformity of N doping must be confirmed in large-area mobility mapping of NDG samples⁷⁵. Moreover, most experimental NDG FET results have been overshadowed by several additional effects, such as NDG growth and transfer and post-processing during the device fabrication and measurements. More studies employing both experimental and theoretical approaches would help validate these results.

Energy storage: batteries

Renewable energy generation and electric vehicles require high-capacity, fast-charging batteries. Since discovering monolayer graphene in 2004, 2D materials and their 3D networks have attracted broad interest as alternatives to bulk graphite or graphitic carbon-based hybrid flakes/sheets¹⁰⁸. However, the current research/applications of battery applications are dominated by powdered-form graphene/graphene derivatives and other carbon-based nanomaterials (e.g., carbon nanotubes, carbon fibers, and carbon black) and hybrids and composites based on these materials^{8,63}. As a battery material, 2D graphene has been overshadowed by other materials with different shapes, sizes, defects, and impurities^{33,57,72,114}.

According to some reports, pristine graphene cannot be applied as the anode in magnesium- or potassium-ion batteries because it has poor adsorption ability^{88,115}. The hexagonal carbon sheet of graphene presents a high-energy barrier to the solid diffusion process required in battery processes because graphene sheets are closely stacked, and their performance is limited at high voltages. Conversely, N doping alters the electronic structure of graphene and produces active sites in the graphene/graphite lattice while increasing the interlayer distance^{19,88,116}. Thus, NDG as the anode material enhances the battery capacity by improving the adsorption, substitution, and intercalation capabilities^{19,53,88}.

Batteries based on CVD-grown NDG are rarely reported^{53,117}. Reddy et al. studied the reversible Li-ion intercalation properties in a Li-ion battery (LIB) assembly using directly grown NDG ($N = 9 \text{ at. \%}$) or graphene on a Cu current collector (Fig. 10)⁵³. The reversible discharge capacity of the NDG-based LIB was almost double that of the graphene-based LIB. They emphasized that the higher capacity resulted from the surface defects introduced via N doping. Moreover, the direct growth process ensured good electrical contact between the NDG electrode and the current

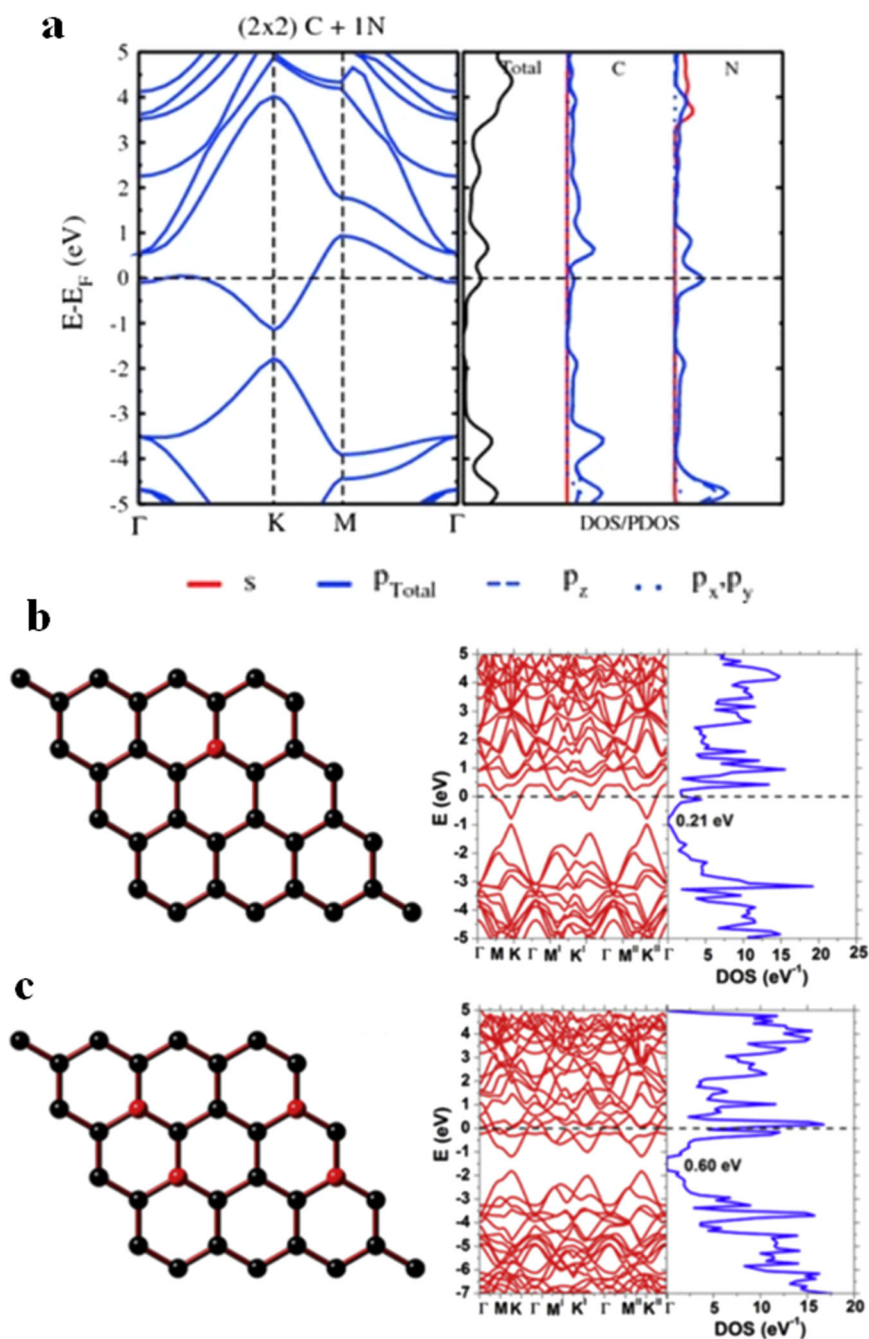


Fig. 9 Density functional theory results. **a** Energy band structure and density of states of NDG (reproduced from¹¹² with permission from Springer Nature); **b, c** optimized structures, energy band structures, and density of states of NDG at different N concentrations (3.13 and 12.50 at.%). Red and black balls represent N and C atoms, respectively (reproduced from¹¹³ with permission from Elsevier).

collector. This assembly reduced the electronic resistance and enhanced the electrode rate capability⁵³.

Because Li is neither abundant nor well distributed in the Earth's crust, it is considerably more expensive than other Earth-abundant alkali metals (Na and K) and Al. Moreover, the demand for batteries is expected to increase in the future. Accordingly, the research focus in the past decade has shifted to Na, K, and Al batteries^{118,119}. Share et al. demonstrated high K-ion storage capacity in K-ion batteries (KIBs) with few-layer NDG as the anode material¹⁸⁸. More specifically, the maximum theoretical storage capacity increased from 278 mA h/g in the graphite-based KIB to 350 mA h/g in the KIB based on N-doped few-layered graphene. The higher capacity of N-doped few-layer graphene than that of

pristine few-layer graphene was attributed to the defective N-doping sites and formation of the first-stage intercalation compound (KC_8). The pyridinic-N configuration imposes a local electron deficiency that draws electrons from nearby K atoms, enhancing KIB storage properties¹⁹.

Thus, N doping can overcome the anode limitations in batteries by providing additional active sites and increasing the storage capacity^{88,116}. The NDG with pyrrolic-N and pyridinic-N configurations is suitable for LIBs and KIBs^{19,53}, but precisely controlling the configuration, distribution, and doping content of N over large areas is a difficult task. In addition, defects and distortions are inevitably introduced by the NDG synthesis process^{34,35}. Although these defects decrease the mobility of NDG, they are beneficial for

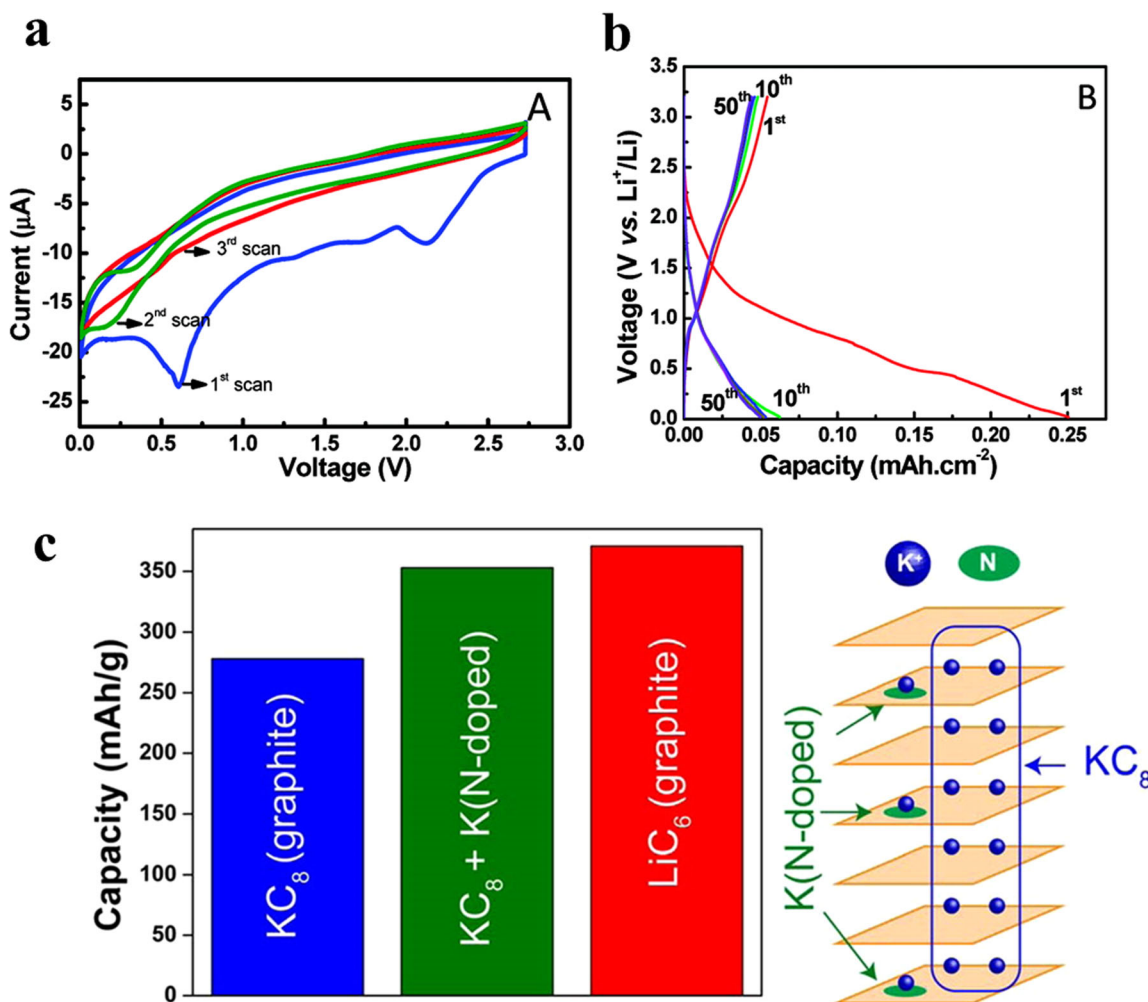


Fig. 10 Electrochemical performance. **a** Cyclic Li-ion battery voltammograms of the NDG/Cu foil electrode and **b** charge/discharge voltage profiles for the NDG electrode (reproduced from⁵³ with permission from the American Chemical Society); **c** K-ion battery: capacity comparison of graphene, NDG, and graphite in battery cells, with a schematic of the staging and defect storage mechanism in few-layer NDG (reproduced from⁸⁸ with permission from the American Chemical Society).

the catalytic reaction in LIBs⁵³. Controlled NDG growth on porous substrates (catalytic or noncatalytic) could be the way forward for large-scale battery applications⁷².

The electrode materials of alkali-metal-ion batteries can be evaluated via DFT simulations. The insertion voltage of alkali-metal atoms in electrode materials and the diffusion barrier and diffusion path of alkali-metal atoms on the structure can be investigated through the DFT. Moreover, the theoretical capacity of the electrode material can be determined by studying the maximum number of alkali-metal atoms adsorbed on the structure. Cao et al.¹²⁰ theoretically investigated the adsorption mechanisms of Li atoms on pyridinic-N, pyrrolic-N, and graphitic-N-type NDG. The adsorption energy of Li atoms was the highest for pyridinic-N (~40% higher than that for pristine graphene). In this configuration, the formation of Li clusters was limited, and the storage capacity was boosted to 1262 mA h/g.

Yu et al. also studied different NDG configurations as the electrode material for LIBs (Fig. 11a)¹⁰⁵. Their results indicate that not all N-doping configurations can increase the capacity of LIBs. On N-substituted graphene, the adsorption energy of a Li atom is positive, meaning that this NDG configuration is an unsuitable electrode material for LIBs. In contrast, N-modified single- or double-vacancy defects, especially pyridinic-N₂V₂ defects, can significantly increase the reversible battery capacity. Therefore,

pyridinic-N and pyrrolic-N-doped configurations are promising electrode materials for LIBs and can improve the performance of Na-ion batteries. Kimal et al.¹²¹ investigated the performance of different types of NDG as the Na-ion battery. They found that after adsorbing six Na atoms, all NDG configurations and pristine graphene become asymmetric, and the adsorption configurations significantly change (Fig. 11b). Furthermore, the Na storage capacity in pyridinic-N or pyrrolic-N-doped graphene is improved by the electron effect originating from the vacancy sites or electron-deficient dopants (Fig. 11b).

Overall, this review can guide performance improvement in CVD-grown NDG in FET and battery applications. For example, graphitic-N can maintain high carrier mobility in FET devices, whereas pyridinic-N and pyrrolic-N types of NDG are essential in batteries.

SUMMARY AND PERSPECTIVES

A good number of articles on the growth and application of NDG have been published in recent years. In addition, several synthesis and characterization techniques have been investigated. However, the literature reveals considerable differences in the properties and device efficiencies of NDG films. Many recent studies have been performed on 3D networks of 2D-doped graphene flakes,

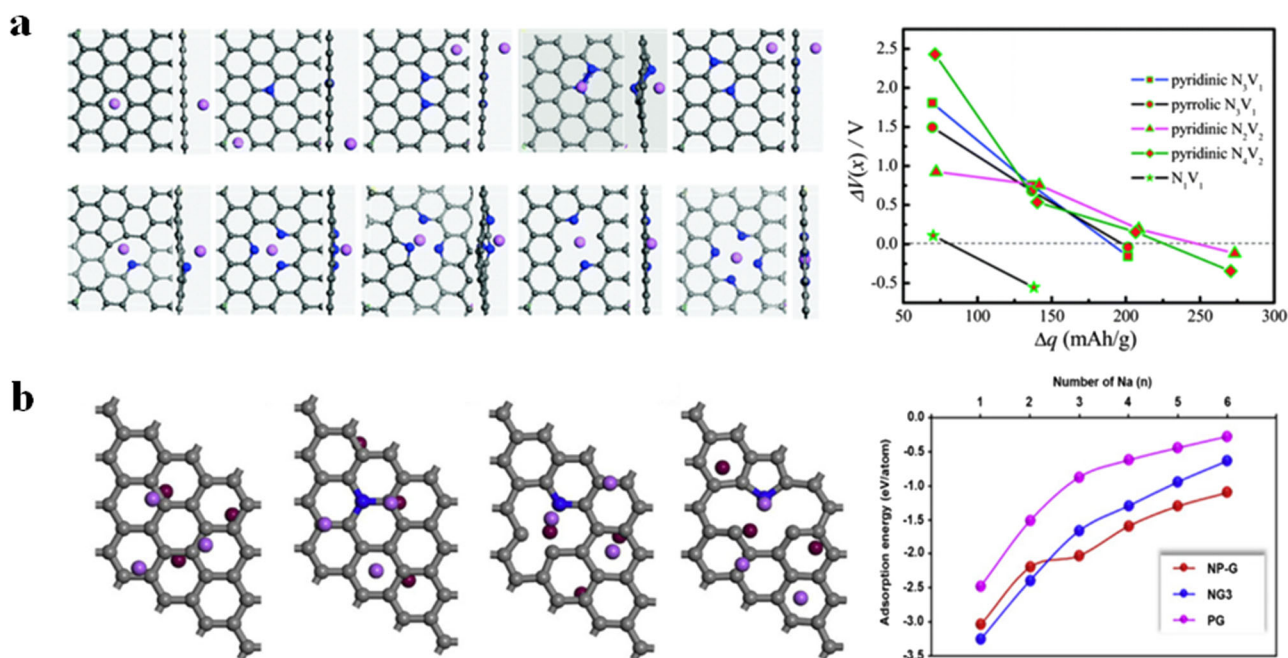


Fig. 11 Computational results of NDG in battery applications. **a** Optimized structures of a Li atom adsorbed on pristine graphene and N-substituted graphene (N_1 , N^{AA}_2 , N^{AB}_2 , N^{AB}_2) N_1V_1 , pyridinic- N_3V_1 , pyrrolic- N_3V_1 , pyridinic- N_2V_2 , and pyridinic- N_4V_2 defects, where N_xV_y denotes a configuration with x N atoms and y vacancies in graphene. The gray, blue, and pink balls represent C, N, and Li atoms, respectively (reproduced from¹⁰⁵ with permission from the Royal Society of Chemistry). **b** Optimized structures of six Na atoms adsorbed on pristine graphene and graphitic-N, pyridinic-N, and pyrrolic-N-type NDG. (reproduced from¹²¹ with permission from Elsevier).

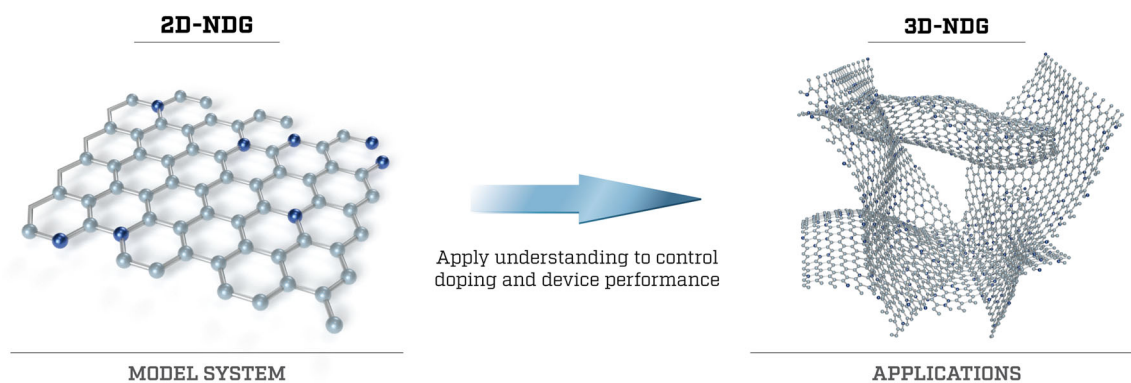


Fig. 12 Schematic illustration. Two-dimensional N-doped graphene (2D NDG) system that can be used as a model to control the N-doping at. %, location, and device performance effects (field-effect transistor). The results could be applied to control N-doping processes and device performance of 3D-NDG materials (e.g., electrochemistry applications).

which contain a variety of undetermined defects and doping sites. As reviewed, well-defined doping configurations N at.% quantities are difficult to obtain, explaining the widely disparate results in the field. Ideally, before proceeding to 3D, the NDG materials should be thoroughly studied in their 2D form in order to understand the underlying formation mechanisms and role of each N-doping configuration and their useful concentration threshold for a given application. However, a method to produce a wafer-scale with a controlled number of NDG layers and uniform N doping is lacking. Among the possible options, CVD is the most promising to overcome this challenge.

The key advantages of the 2D form of NDG are as follows: (i) easy and reliable control of N doping; (ii) unambiguous characterization of C–N bonding types using either XPS or TEM techniques; and (iii) avoidance of the effect of N inclusion at the interlayer (intercalation) or voids or at functional/defect sites, such as that of 2D networks of 3D graphene. In future work, we

recommend CVD-grown 2D NDG as a model system (Fig. 12) for controlling the N-doping level and configuration, to understand and engineer the doping effects in target applications. Moreover, these studies could be highly beneficial when implementing 3D networks of 2D NDG (Fig. 12) for particular applications (e.g., electrochemistry) and interpreting device performance.

We recommend the following critical pathways for CVD-based NDG growth:

- Growth

The development of a standard growth process would help achieve controlled growth of high-quality NDG at the wafer-scale. Thus far, the process parameters and activation sources of NDG growth in the literature are widely variable. Pretreated catalytic substrates (e.g., Cu, Ni, or Cu/Ni alloy) under a proper C or N source prior to graphene growth to precisely

control the C and N quantities need to be researched in greater detail.

Limited substrates (catalytic and dielectric) for NDG growth have been explored thus far. Various other substrates (e.g., GaN for photodetector applications) must be studied.

The vacancies created via doping, especially those in pyridinic and pyrrolic-N, must be controlled, and their effects on applications must be studied and modeled simultaneously.

Once NDG growth over squared centimeter samples with controlled quality is achieved, large-area graphene growth CVD systems (e.g., roll-to-roll CVD systems) could be adapted to achieve wafer-scale NDG growth.

● Characterization

Both global and local characterization techniques are required to determine the quality of the as-produced NDG material. In some reports, this complementarity is overlooked compromising the quality of the analytical study and subsequent conclusions.

Experimental and theoretical studies of each type of N-doping configuration and its effect on target applications are required. For example, in FET applications, whether 2 at.% of N, predominantly of graphitic-N-type, opens a suitable bandgap while retaining the requisite of high charge carrier mobility must be determined.

● Applications

To achieve reliable and reproducible results for 3D constructs, first, the properties (e.g., electrical, optical, and mechanical) and applications (e.g., FET, battery, sensing, and catalysis) of NDG in the 2D form must be explored in greater detail.

The N-dopant location (substitutional or intercalated) in multi-layer NDG and its effect on the performance of a specific application (e.g., battery) must also be explored in greater detail.

These studies would facilitate the adoption of NDG as an active material for nanoelectronics, energy storage devices, and many other technologies. Then, and thinking beyond this, 3D networks of NDG could be assembled with better control and reproducible responses.

DATA AVAILABILITY

All relevant data are available from the corresponding author.

Received: 19 July 2021; Accepted: 20 January 2022;

Published online: 04 March 2022

REFERENCES

- Morozov, S. V. et al. Giant intrinsic carrier mobilities in graphene and its bilayer. *Phys. Rev. Lett.* **100**, 016602 (2008).
- Balandin, A. A., Ghosh, S., Nika, D. L. & Pokatilov, E. P. Thermal conductivity of graphene: the first measurements and theoretical analysis. *Therm. Cond.* **30**, 97 (2010).
- Stoller, M. D., Park, S. J., Zhu, Y. W., An, J. H. & Ruoff, R. S. Graphene-based ultracapacitors. *Nano Lett.* **8**, 3498–3502 (2008).
- Deokar, G. et al. Wafer-scale few-layer graphene growth on Cu/Ni films for gas sensing applications. *Sensor Actuat B-Chem.* **305**, 127458 (2020).
- Penezic, A. et al. Carbohydrate-lectin interaction on graphene-coated surface plasmon resonance (SPR) interfaces. *Plasmonics* **9**, 677–683 (2014).
- He, Q. Y., Wu, S. X., Yin, Z. Y. & Zhang, H. Graphene-based electronic sensors. *Chem. Sci.* **3**, 1764–1772 (2012).
- Novodchuk, I., Bajcsy, M. & Yavuz, M. Graphene-based field effect transistor biosensors for breast cancer detection: a review on biosensing strategies. *Carbon* **172**, 431–453 (2021).

- Huang, X., Zeng, Z. Y., Fan, Z. X., Liu, J. Q. & Zhang, H. Graphene-based electrodes. *Adv. Mater.* **24**, 5979–6004 (2012).
- Wei, W. et al. Graphene FETs with aluminum bottom-gate electrodes and its natural oxide as dielectrics. *IEEE Trans. Electron Dev.* **62**, 2769–2773 (2015).
- Bi, L. Q., Dai, S. S., Wu, Y. B. & Guo, D. H. Graphene field effect transistors and their applications in terahertz technology: a review. *Carbon* **145**, 772–772 (2019).
- Bae, S. et al. Roll-to-roll production of 30-inch graphene films for transparent electrodes. *Nat. Nanotechnol.* **5**, 574–578 (2010).
- Chen, Y., Li, J. Z., Li, T., Zhang, L. K. & Meng, F. B. Recent advances in graphene-based films for electromagnetic interference shielding: review and future prospects. *Carbon* **180**, 163–184 (2021).
- Hossain, S. et al. Nanostructured graphene materials utilization in fuel cells and batteries: a review. *J. Energy Storage* **29**, 101386 (2020).
- Yang, W. et al. Nitrogen plasma modified CVD grown graphene as counter electrodes for bifacial dye-sensitized solar cells. *Electrochim. Acta* **173**, 715–720 (2015).
- Qiu, Y. C. et al. High-rate, ultra long cycle-life lithium/sulfur batteries enabled by nitrogen-doped graphene. *Nano Lett.* **14**, 4821–4827 (2014).
- Cai, D. D. et al. Superhigh capacity and rate capability of high-level nitrogen-doped graphene sheets as anode materials for lithium-ion batteries. *Electrochim. Acta* **90**, 492–497 (2013).
- Xu, W. et al. N-doped graphene field-effect transistors with enhanced electron mobility and air-stability. *Small* **10**, 1999–2005 (2014).
- Liu, H. T., Liu, Y. Q. & Zhu, D. B. Chemical doping of graphene. *J. Mater. Chem.* **21**, 3335–3345 (2011).
- Wu, X. et al. Advanced carbon-based anodes for potassium-ion batteries. *Adv. Energy Mater.* **9**, 1900343 (2019).
- Ikram, R. et al. Recent advancements of N-doped graphene for rechargeable batteries: a review. *Crystals* **10**, 1, (2020).
- He, C. Y., Wang, R. H., Fu, H. G. & Shen, P. K. Nitrogen-self-doped graphene as a high capacity anode material for lithium-ion batteries. *J. Mater. Chem. A* **1**, 14586–14591 (2013).
- López-Urías, F., Lv, R., Terrones, H. & Terrones, M. Doped Graphene: Theory, Synthesis, Characterization, and Applications. <https://doi.org/10.1002/9781118691281.ch9>. In book: Graphene Chemistry (pp.183–207). https://www.researchgate.net/publication/277705007_Doped_Graphene_Theory_Synthesis_Characterization_and_Applications (2013).
- Lee, S. J. et al. Heteroatom-doped graphene-based materials for sustainable energy applications: a review. *Renew. Sust. Energ. Rev.* **143**, 110849 (2021).
- Lee, H., Paeng, K. & Kim, I. S. A review of doping modulation in graphene. *Synth. Met.* **244**, 36–47 (2018).
- Wang, X. N-doping of graphene through electrothermal reactions with ammonia. *Science* **329**, 1467–1467 (2010).
- Son, M. et al. High-quality nitrogen-doped graphene films synthesized from pyridine via two-step chemical vapor deposition. *Carbon* **159**, 579–585 (2020).
- Late, D. J. et al. Characteristics of field-effect transistors based on undoped and B- and N-doped few-layer graphenes. *Solid State Commun.* **150**, 734–738 (2010).
- Ma, X. L., Ning, G. Q., Qi, C. L., Xu, C. G. & Gao, J. S. Phosphorus and nitrogen dual-doped few-layered porous graphene: a high-performance anode material for lithium-ion batteries. *ACS Appl. Mater. Inter.* **6**, 14415–14422 (2014).
- Zhou, J. H. et al. Growth and properties of large-area sulfur-doped graphene films. *J. Mater. Chem. C* **5**, 7944–7949 (2017).
- Kalita, G., Wakita, K., Takahashi, M. & Umeno, M. Iodine doping in solid precursor-based CVD growth graphene film. *J. Mater. Chem.* **21**, 15209–15213 (2011).
- Feng, W., Long, P., Feng, Y. & Li, Y. Two-dimensional fluorinated graphene: synthesis, structures, properties and applications. *Adv. Sci.* **3**, 1500413 (2016).
- Granzier-Nakajima, T., Fujisawa, K., Anil, V., Terrones, M. & Yeh, Y. T. Controlling nitrogen doping in graphene with atomic precision: synthesis and characterization. *Nanomaterials* **9**, 425 (2019).
- Wang, H. B., Maiyalagan, T. & Wang, X. Review on recent progress in nitrogen-doped graphene: synthesis, characterization, and its potential applications. *ACS Catal.* **2**, 781–794 (2012).
- Zhai, Z. H., Shen, H. L., Chen, J. Y., Li, X. M. & Jiang, Y. Direct growth of nitrogen-doped graphene films on glass by plasma-assisted hot filament CVD for enhanced electricity generation. *J. Mater. Chem. A* **7**, 12038–12049 (2019).
- Gao, H. et al. A simple method to synthesize continuous large area nitrogen-doped graphene. *Carbon* **50**, 4476–4482 (2012).
- Sturala, J., Luxa, J., Pumera, M. & Sofer, Z. Chemistry of graphene derivatives: syntheses, applications, and perspectives. *Chemistry* **24**, 5992–6006 (2018).
- Plutnar, J., Pumera, M. & Sofer, Z. The chemistry of CVD graphene. *J. Mater. Chem. C* **6**, 6082–6101 (2018).
- Terrones, H., Lv, R. T., Terrones, M. & Dresselhaus, M. S. The role of defects and doping in 2D graphene sheets and 1D nanoribbons. *Rep. Prog. Phys.* **75**, 062501 <https://doi.org/10.1088/0034-4885/75/6/062501> (2012).

39. Olanrele, S. O., Lian, Z., Si, C. W. & Li, B. Halogenation of graphene triggered by heteroatom doping. *Rsc Adv.* **9**, 37507–37511 (2019).
40. Karlicky, F., Datta, K. K. R., Otyepka, M. & Zboril, R. Halogenated graphenes: rapidly growing family of graphene derivatives. *Acs Nano* **7**, 6434–6464 (2013).
41. Kashid, R. V. et al. Field emission characteristics of pristine and N-doped graphene measured by in-situ transmission electron microscopy. *J. Appl. Phys.* **113**, 214311 (2013).
42. Karimzadeh, A., Hasanzadeh, M., Shadjou, N. & de la Guardia, M. Optical bio (sensing) using nitrogen doped graphene quantum dots: recent advances and future challenges. *Trac Trend Anal. Chem.* **108**, 110–121 (2018).
43. Wang, Y., Shao, Y. Y., Matson, D. W., Li, J. H. & Lin, Y. H. Nitrogen-doped graphene and its application in electrochemical biosensing. *Acs Nano* **4**, 1790–1798 (2010).
44. Feng, S. M. et al. Ultrasensitive molecular sensor using N-doped graphene through enhanced Raman scattering. *Sci. Adv.* **2**, e1600322 (2016).
45. Wang, R. et al. Preparation of nitrogen-doped TiO₂/graphene nanohybrids and application as counter electrode for dye-sensitized solar cells. *Acs Appl. Mater. Inter.* **6**, 2118–2124 (2014).
46. Luo, Z. Q. et al. Pyridinic N doped graphene: synthesis, electronic structure, and electrocatalytic property. *J. Mater. Chem.* **21**, 8038–8044 (2011).
47. Zhao, Y., Nakamura, R., Kamiya, K., Nakanishi, S. & Hashimoto, K. Nitrogen-doped carbon nanomaterials as non-metal electrocatalysts for water oxidation. *Nat. Commun.* **4**, 2390 (2013).
48. Liu, X. & Dai, L. M. Carbon-based metal-free catalysts. *Nat. Rev. Mater.* **1**, 16064 (2016).
49. Bagley, J. D., Kumar, D. K., See, K. A. & Yeh, N. C. Selective formation of pyridinic-type nitrogen-doped graphene and its application in lithium-ion battery anodes. *Rsc Adv.* **10**, 39562–39571 (2020).
50. Chu, F. Q. et al. Nitrogen-doped three-dimensional graphene-supported platinum catalysts for polymer electrolyte membrane fuel cells application. *Funct. Mater. Lett.* **11**, 1850015 (2018).
51. Wang, K. W. et al. In situ grown monolayer N-Doped graphene and ZnO on ZnFe₂O₄ hollow spheres for efficient photocatalytic tetracycline degradation. *Colloid Surface A* **618**, 126362 (2021).
52. Bie, C. B., Zhu, B. C., Xu, F. Y., Zhang, L. Y. & Yu, J. G. In situ grown monolayer N-doped graphene on CdS hollow spheres with seamless contact for photocatalytic CO₂ reduction. *Adv. Mater.* **31**, 1902868 (2019).
53. Reddy, A. L. M. et al. Synthesis of nitrogen-doped graphene films for lithium battery application. *Acs Nano* **4**, 6337–6342 (2010).
54. Kaur, M., Kaur, M. & Sharma, V. K. Nitrogen-doped graphene and graphene quantum dots: a review on synthesis and applications in energy, sensors and environment. *Adv. Colloid Interfac.* **259**, 44–64 (2018).
55. Chen, Z. Y. et al. Nitrogen-doped interpenetrating porous carbon/graphene networks for supercapacitor applications. *Chem. Eng. J.* **409**, 127891 (2021).
56. Wei, D. et al. Synthesis of N-doped graphene by chemical vapor deposition and its electrical properties. *Nano Lett.* **9**, 1752–1758 (2009).
57. Yadav, R. & Dixit, C. K. Synthesis, characterization and prospective applications of nitrogen-doped graphene: a short review. *J. Sci. Adv. Mater. Dev.* **2**, 141–149 (2017).
58. Capasso, A. et al. Nitrogen-doped graphene films from chemical vapor deposition of pyridine: influence of process parameters on the electrical and optical properties. *Beilstein J. Nanotech.* **6**, 2028–2038 (2015).
59. Bie, C. B. et al. Design, fabrication, and mechanism of nitrogen-doped graphene-based photocatalyst. *Adv. Mater.* **33**, 2003521 (2021).
60. Alazmi, A., Rasul, S., Patole, S. P. & Costa, P. M. F. J. Comparative study of synthesis and reduction methods for graphene oxide. *Polyhedron* **116**, 153–161 (2016).
61. Maddi, C. et al. Nano-architecture of nitrogen-doped graphene films synthesized from a solid CN source. *Sci Rep.* **8**, 3247 (2018).
62. Lin, Z. Y., Waller, G. H., Liu, Y., Liu, M. L. & Wong, C. P. 3D Nitrogen-doped graphene prepared by pyrolysis of graphene oxide with polypyrrole for electrocatalysis of oxygen reduction reaction. *Nano Energy* **2**, 241–248 (2013).
63. Zhang, Z. et al. Verifying the rechargeability of Li-CO₂ batteries on working cathodes of Ni nanoparticles highly dispersed on N-doped graphene. *Adv. Sci.* **5**, 1700567 (2018).
64. Pham, T. V. et al. High areal capacitance of N-doped graphene synthesized by Arc discharge. *Adv. Funct. Mater.* **29**, 1905511 (2019).
65. Panchokarla, L. S. et al. Synthesis, structure, and properties of boron- and nitrogen-doped graphene. *Adv. Mater.* **21**, 4726 (2009).
66. Sun, L. et al. Nitrogen-doped graphene with high nitrogen level via a one-step hydrothermal reaction of graphene oxide with urea for superior capacitive energy storage. *Rsc Adv.* **2**, 4498 (2012).
67. Long, D. H. et al. Preparation of nitrogen-doped graphene sheets by a combined chemical and hydrothermal reduction of graphene oxide. *Langmuir* **26**, 16096–16102 (2010).
68. Bai, J. C. et al. Nitrogen-doped graphene as catalysts and catalyst supports for oxygen reduction in both acidic and alkaline solutions. *Int. J. Hydrog. Energ.* **38**, 1413–1418 (2013).
69. Deng, D. H. et al. Toward N-doped graphene via solvothermal synthesis. *Chem. Mater.* **23**, 1188–1193 (2011).
70. Zhang, L. L. et al. Single nickel atoms on nitrogen-doped graphene enabling enhanced kinetics of lithium-sulfur batteries. *Adv. Mater.* **31**, 1903955 (2019).
71. Xu, H. F., Ma, L. B. & Jin, Z. Nitrogen-doped graphene: synthesis, characterizations and energy applications. *J. Energy Chem.* **27**, 146–160 (2018).
72. Ullah, S. et al. Synthesis of doped porous 3D graphene structures by chemical vapor deposition and its applications. *Adv. Funct. Mater.* **29**, 1904457 (2019).
73. Deokar, G. et al. Semi-transparent graphite films growth on Ni and their double-sided polymer-free transfer. *Sci. Rep.* **10**, 14703 (2020).
74. Deokar, G., Genovese, A. & Costa, P. Fast, wafer-scale growth of a nanometer-thick graphite film on Ni foil and its structural analysis. *Nanotechnology* **31**, 485605 (2020).
75. Deokar, G. et al. Towards high quality CVD graphene growth and transfer. *Carbon* **89**, 82–92 (2015).
76. Fiori, S. et al. “Inside out” growth method for high-quality nitrogen-doped graphene. *Carbon* **171**, 704–710 (2021).
77. Shi, B. et al. One-pot green synthesis of oxygen-rich nitrogen-doped graphene quantum dots and their potential application in pH-sensitive photoluminescence and detection of mercury(II) ions. *Talanta* **142**, 131–139 (2015).
78. Balamurugan, J., Nguyen, T. T., Aravindan, V., Kim, N. H. & Lee, J. H. Flexible solid-state asymmetric supercapacitors based on nitrogen-doped graphene encapsulated ternary metal-nitrides with ultralong cycle life. *Adv. Funct. Mater.* **28**, 1804663 (2018).
79. Lin, Y. P. et al. Efficient and low-damage nitrogen doping of graphene via plasma-based methods. *Carbon* **100**, 337–344 (2016).
80. Yanilmaz, A. et al. Nitrogen doping for facile and effective modification of graphene surfaces. *Rsc Adv.* **7**, 28383–28392 (2017).
81. Rybin, M. et al. Efficient nitrogen doping of graphene by plasma treatment. *Carbon* **96**, 196–202 (2016).
82. Wei, D. C. et al. Low temperature critical growth of high quality nitrogen doped graphene on dielectrics by plasma-enhanced chemical vapor deposition. *Acs Nano* **9**, 164–171 (2015).
83. Liu, B., Yang, C. M., Liu, Z. W. & Lai, C. S. N-doped graphene with low intrinsic defect densities via a solid source doping technique. *Nanomaterials* **7**, 302 (2017).
84. Lv, R. et al. Nitrogen-doped graphene: beyond single substitution and enhanced molecular sensing. *Sci. Rep.* **2**, 586 (2012).
85. Li, J. Y. et al. Scalable synthesis of pyrrolic N-doped graphene by atmospheric pressure chemical vapor deposition and its terahertz response. *Carbon* **62**, 330–336 (2013).
86. Ito, Y. et al. Chemical vapor deposition of N-doped graphene and carbon films: the role of precursors and gas phase. *Acs Nano* **8**, 3337–3346 (2014).
87. Jin, Z., Yao, J., Kittrell, C. & Tour, J. M. Large-scale growth and characterizations of nitrogen-doped monolayer graphene sheets. *ACS Nano* **5**, 4112–4117 (2011).
88. Share, K., Cohn, A. P., Carter, R., Rogers, B. & Pint, C. L. Role of nitrogen-doped graphene for improved high-capacity potassium ion battery anodes. *Acs Nano* **10**, 9738–9744 (2016).
89. Bao, J. F., Kishi, N. & Soga, T. Synthesis of nitrogen-doped graphene by the thermal chemical vapor deposition method from a single liquid precursor. *Mater. Lett.* **117**, 199–203 (2014).
90. Prasanthi, T. N., Sudha, C., Saroja, S. & Vijayalakshmi, M. Diffusion of nitrogen in FCC-Fe and FCC-Ni lattices: molecular dynamic simulations. In *11th International Conference on High Nitrogen Steels* (Indian Institute of Metals, 2012).
91. Deng, B., Liu, Z. F. & Peng, H. L. Toward mass production of CVD graphene films. *Adv. Mater.* **31**, 1800996 (2019).
92. Yang, R. T., Goethel, P. J., Schwartz, J. M. & Lund, C. R. F. Solubility and diffusivity of carbon in metals. *J. Catal.* **122**, 206–210 (1990).
93. Li, X. S., Cai, W. W., Colombo, L. & Ruoff, R. S. Evolution of graphene growth on Ni and Cu by carbon isotope labeling. *Nano Lett.* **9**, 4268–4272 (2009).
94. Reina, A. et al. Large area, few-layer graphene films on arbitrary substrates by chemical vapor deposition. *Nano Lett.* **9**, 30–35 (2009).
95. Deokar, G., Codron, J.-L., Boyaval, C., Wallart, X. & Vignaud, D. In *4th Graphene Conference, Graphene 2014* (2014).
96. Prasanthi, T. N., Sudha, C., Saroja, S. & Vijayalakshmi, M. Simulation of nitrogen diffusion in Ni vis-a-vis Fe - Identification of better structural material for neutron detectors. *Results Phys.* **4**, 96–100 (2014).
97. Zhang, C. H. et al. Synthesis of nitrogen-doped graphene using embedded carbon and nitrogen sources. *Adv. Mater.* **23**, 1020–1024 (2011).
98. Joucken, F. et al. Charge transfer and electronic doping in nitrogen-doped graphene. *Sci. Rep.* **5**, 14564 (2015).

99. Zan, R. & Altuntepe, A. Nitrogen doping of graphene by CVD. *J. Mol. Struct.* **1199**, 127026 (2020).
100. Ferrari, A. C. et al. Raman spectrum of graphene and graphene layers. *Phys. Rev. Lett.* **97**, 187401 (2006).
101. Ferrari, A. C. Raman spectroscopy of graphene and graphite: disorder, electron-phonon coupling, doping and nonadiabatic effects. *Solid State Commun.* **143**, 47–57 (2007).
102. Pirkle, A. et al. The effect of chemical residues on the physical and electrical properties of chemical vapor deposited graphene transferred to SiO₂. *Appl. Phys. Lett.* **99**, 122108 (2011).
103. Kumar, K., Kim, Y. S. & Yang, E. H. The influence of thermal annealing to remove polymeric residue on the electronic doping and morphological characteristics of graphene. *Carbon* **65**, 35–45 (2013).
104. Wang, X. et al. Heteroatom-doped graphene materials: syntheses, properties and applications. *Chem. Soc. Rev.* **43**, 7067–7098 (2014).
105. Yu, Y. X. Can all nitrogen-doped defects improve the performance of graphene anode materials for lithium-ion batteries? *Phys. Chem. Chem. Phys.* **15**, 16819–16827 (2013).
106. Jalili, S. & Vaziri, R. Study of the electronic properties of Li-intercalated nitrogen doped graphite. *Mol. Phys.* **109**, 687–694 (2011).
107. Callahan, D. J. et al. Triple stimulus-responsive polypeptide nanoparticles that enhance intratumoral spatial distribution. *Nano Lett.* **12**, 4 (2012).
108. Novoselov, K. S. et al. Electric field effect in atomically thin carbon films. *Science* **306**, 666–669 (2004).
109. Buron, J. D. et al. Graphene mobility mapping. *Sci. Rep.* **5**, 12305 (2015).
110. Acharya, S., Babu, A. V., Khadar, R. A. & Kottantharayil, A. Mobility improvement in CVD graphene by using local metal side-gate. *Semicond. Sci. Technol.* **35**, 045027 (2020).
111. Schwierz, F. Graphene transistors. *Nat. Nanotechnol.* **5**, 487–496 (2010).
112. Mukherjee, S. & Kaloni, T. P. Electronic properties of boron- and nitrogen-doped graphene: a first principles study. *J. Nanopart. Res.* **14**, 1059 (2012).
113. Olaniyan, O. et al. A systematic study of the stability, electronic and optical properties of beryllium and nitrogen co-doped graphene. *Carbon* **129**, 207–227 (2018).
114. Xu, J., Jiang, P., Liang, X. L., Tian, R. J. & Liu, Y. M. Nitrogen-doped porous carbon as cathodes for aluminum-ion batteries. *Fuller. Nanotub. Carbon Nanostructures* **29**, 21–27 (2021).
115. Yao, F. et al. Diffusion mechanism of lithium ion through basal plane of layered graphene. *J. Am. Chem. Soc.* **134**, 8646–8654 (2012).
116. Ju, Z. C. et al. Few layer nitrogen-doped graphene with highly reversible potassium storage. *Energy Storage Mater.* **11**, 38–46 (2018).
117. Childress, A. et al. Effect of nitrogen doping in the few layer graphene cathode of an aluminum ion battery. *Chem. Phys. Lett.* **733**, 136669 (2019).
118. Smajic, J. et al. Capacity retention analysis in aluminum-sulfur batteries. *Acs Appl. Energ. Mater.* **3**, 6805–6814 (2020).
119. Smajic, J. et al. Mesoporous reduced graphene oxide as a high capacity cathode for aluminum batteries. *Small* **14**, 1803584 (2018).
120. Ma, C., Shao, X. & Cao, D. Nitrogen-doped graphene nanosheets as anode materials for lithium ion batteries: a first-principles study. *J. Mater. Chem.* **22**, 8911–8915 (2012).

121. Wasalathilake, K. C., Ayoko, G. A. & Yan, C. Effects of heteroatom doping on the performance of graphene in sodium-ion batteries: A density functional theory investigation. *Carbon* **140**, 276–285 (2018).

ACKNOWLEDGEMENTS

This work was supported by KAUST (REI/1/4258-01-01). We are thankful to KAUST editing services for their contribution to technical English-language editing. The figure in Fig. 1, Fig. 2, and Fig. 12 were illustrated by Xavier Pita, a scientific illustrator at KAUST.

AUTHOR CONTRIBUTIONS

GD: Literature survey, conceptualization, original draft, writing (review and editing), **JJ:** DFT part literature survey, writing and editing, **US:** Supervision, writing (review and editing), project administration, funding acquisition, **PMFJC:** Supervision, writing (review and editing), project administration, funding acquisition.

COMPETING INTERESTS

The authors declare no competing interests.

ADDITIONAL INFORMATION

Correspondence and requests for materials should be addressed to Geetanjali Deokar.

Reprints and permission information is available at <http://www.nature.com/reprints>

Publisher's note Springer Nature remains neutral with regard to jurisdictional claims in published maps and institutional affiliations.



Open Access This article is licensed under a Creative Commons Attribution 4.0 International License, which permits use, sharing, adaptation, distribution and reproduction in any medium or format, as long as you give appropriate credit to the original author(s) and the source, provide a link to the Creative Commons license, and indicate if changes were made. The images or other third party material in this article are included in the article's Creative Commons license, unless indicated otherwise in a credit line to the material. If material is not included in the article's Creative Commons license and your intended use is not permitted by statutory regulation or exceeds the permitted use, you will need to obtain permission directly from the copyright holder. To view a copy of this license, visit <http://creativecommons.org/licenses/by/4.0/>.

© The Author(s) 2022